

Appendix F

N92-14908<sup>119</sup>

## Sources of Noise in Magneto-Optical Readout

M. Mansuripur

Optical Sciences Center

University of Arizona

In this document we analyze the various sources of noise which are often encountered in magneto-optical readout systems. Although the focus is on magneto-optics, most sources of noise are common among the various optical recording systems and one can easily adapt the results of this work to other media and systems. A description of the magneto-optical readout system under consideration is given in Section 1; also described there are the standard methods and the relevant terminology of signal and noise measurement. After these preliminary considerations, the characteristics of thermal noise, which originates in the electronic circuitry of readout, are described in Section 2. In Section 3 we consider the most fundamental of all sources of noise, the shot noise, and give a detailed account of its statistical properties. Shot noise, which is due to random fluctuations in photon arrival times, is an ever-present noise in optical detection. Since the performance of magneto-optical recording devices in use today is approaching the limit imposed by the shot noise, it is important that the reader have a good grasp of this particular source of noise. In Section 4 we describe a model for the laser noise, and present measurement results which yield numerical values for the strength of the laser power fluctuations. Spatial variations of the disk reflectivity and random depolarization phenomena also contribute to the overall level of noise in readout; these and related issues are treated in Section 5. The final section is devoted to numerical simulation results, describing some of the more frequently encountered sources of noise which accompany the recorded waveform itself, namely, jitter noise and signal-amplitude-fluctuation noise.

1. **Preliminaries :** Throughout this chapter, frequent reference will be made to the readout system depicted in Fig. 1. The light source in this system is a semiconductor diode laser which operates at a constant (CW) output power level†. The reflected light from the magneto-optical disk consists of a polarization component parallel to the direction of incident polarization  $X$ , and a perpendicular component  $Y$ , which carries information about the recorded data.

For the purpose of monitoring the laser power fluctuations, the leaky polarizing-beam-splitter directs a small fraction  $\gamma^2$  of the emitted light towards a photodetector; the output of this detector is fed back to the laser in order to stabilize its radiation level. The light transmitted by the leaky PBS is linearly polarized along  $X$  but, upon reflection from the disk, it acquires a  $Y$ -component as well. In the return path, the leaky PBS provides the detection module with a fraction  $\gamma$  of the  $X$ -component as well as the entire  $Y$ -component. The latter is the magneto-optically generated signal which carries the desired information; the former, although barren of such information, is needed in the scheme of differential detection in order to properly extract the data.

To eliminate the ellipticity of the beam, a phase compensator (either quarter-wave plate or adjustable Soleil-Babinet retarder) is employed. A regular PBS, with its axes at  $45^\circ$  to  $X$  and  $Y$ , together with detectors #1 and #2 comprise a balanced differential detection module. These detectors are low-noise, photodiode/preamplifier integrated circuits whose outputs are fed to a differential amplifier for subtraction and further amplification.

Let us now describe the units of signal and noise which are commonly used in practical measurements. A constant (DC) voltage  $V$  or current  $I$  is specified in terms of the power  $P$  that it delivers to a fixed resistor  $R$ , that is,  $P = V^2/R$  or  $P = RI^2$ . The standard value of  $R$  is  $50 \Omega$  and the power thus measured may be stated either in Watts or in milliWatts. In the logarithmic units known

---

† For the purpose of noise reduction in practice the laser drive current is modulated at a frequency in the range of several hundred MHz. Generally, the modulation frequency is well beyond the bandwidth of the detection system and is ignored by the detectors. Signal and noise analysis, therefore, may proceed by ignoring the modulation of the laser and treating its beam as CW.

as deciBell (*dB*) the strength of the signal is defined as  $10 \log_{10} P$ ; if  $P$  is in Watts the logarithmic unit is called dBw, and if  $P$  is in milliWatts it is known as dBm. For example, the power of a 1 Volt DC signal is 13 dBm, while that of a 1 Amp DC current is 47 dBm. The same rules and definitions apply to single-frequency (AC) signals, provided of course that one remembers that the effective (root-mean-square) amplitude of a sinusoid is  $1/\sqrt{2}$  times its maximum amplitude.

When the dimensionless ratio of two quantities such as  $P_1/P_2$  or  $V_1/V_2$  or  $I_1/I_2$  is expressed on the logarithmic scale, the units are specified as *dB*. It must be emphasized that the ratio of powers in *dB* is defined as  $10 \log P_1/P_2$ , whereas for currents and voltages the correct definition is  $20 \log (I_1/I_2)$  and  $20 \log (V_1/V_2)$ .

If a signal is amplified prior to the measurement, then the gain  $G$  must also be taken into account. Generally, when one uses a logarithmic scale, one must subtract the value of  $20 \log_{10} G$  from the signal power in order to eliminate the gain factor. It is important here that the gain be dimensionless, that is, voltage be amplified to voltage and current be amplified to current. If, on the other hand, current is amplified to voltage (or vice versa) then the gain must be adjusted to take account of the resistance  $R$ . For instance, if the initial noise current has a power of  $R I^2$ , after amplification (and conversion to voltage) its power will become  $G^2 I^2 / R$ . Therefore, the proper gain coefficient in this instance is not  $G$  but  $G/R$  (where  $R$  is typically  $50 \Omega$ ).

Unlike the signal, noise has a broad spectrum and its strength (or power) depends on the bandwidth within which it is being measured. The spectral density of the noise is usually defined as the average noise power delivered to a  $50 \Omega$  resistor within a bandwidth of 1 Hz, and is denoted by  $R \langle i_n^2 \rangle$  or  $\langle v_n^2 \rangle / R$ , depending on whether the noise is due to fluctuations of current or voltage. We shall denote the rms noise current by  $i_n$ , although formally the appropriate notation is  $\sqrt{\langle i_n^2 \rangle}$ . Similarly the rms noise voltage shall be denoted by  $v_n$ . It is customary in practice to measure the noise power not in a 1 Hz bandwidth, but in a 30 kHz bandwidth, and express the result in dBw or dBm. Thus, a noise current of  $10 \text{ pA}/\sqrt{\text{Hz}}$  will have a power of

$$10 \log_{10}(50 \times 10^{-22} \times 30000) = -158.24 \text{ dBw} = -128.24 \text{ dBm} .$$

Similarly, the measured power of a noise voltage with the spectral density of  $1 \text{ nV}/\sqrt{\text{Hz}}$  will be

$$10 \log_{10}(10^{-18} \times 30000/50) = -152.22 \text{ dBW} = -122.22 \text{ dBm} .$$

In the above example, if one assumes that an amplifier with a gain of  $G = 100 \text{ V/A}$  is used to convert current to voltage, then the normalized gain  $G/R$  will be equal to 2. This means that the noise current must be 6 dB below the level of the noise voltage, as is indeed the case.

2. **Noise in the Electronic Circuitry :** The fluctuating conduction electrons within resistors and transistors of an electronic circuit create a random voltage or current at the circuit's output terminal. When these fluctuations are caused by thermal motion of the electrons the resulting noise is referred to as Johnson noise. A resistor  $R$  at an equilibrium temperature  $T$  exhibits a noise whose spectrum is flat for practically all frequencies of interest. If the Johnson noise of this resistor is measured within a bandwidth  $B$ , the resulting magnitude of the noise current will be

$$\langle i_{th}^2 \rangle = \frac{4 k_B T B}{R} \quad (1)$$

In the above equation the brackets  $\langle \cdot \rangle$  indicate statistical averaging or averaging over time,  $k_B$  is Boltzmann's constant ( $1.38 \times 10^{-23}$  Joule/ $^{\circ}K$ ),  $T$  is the absolute temperature (in degrees Kelvin),  $B$  is the bandwidth (in Hertz), and  $R$  is the resistance (in Ohms). For simplicity's sake we shall denote the root-mean-square value of the noise current by  $i_{th}$  instead of  $\sqrt{\langle i_{th}^2 \rangle}$ . Since the frequency spectrum of thermal noise is flat, one usually specifies the strength of the noise in a 1 Hz bandwidth. Thus the noise amplitude of a 1 k $\Omega$  resistor at room temperature is about 4 pA/ $\sqrt{Hz}$ . If the bandwidth of the measuring system happens to be  $B = 1$  MHz, then the measured noise current will be 4 nA. The corresponding rms noise voltage is then given by  $v_{th} = R i_{th} = 4 \mu V$ .

An amplifier, in addition to multiplying the input noise amplitude by a gain factor, introduces a noise of its own. This is because in transistors, for instance, random generation and recombination of electrons and holes, or the random arrival of these carriers at the collector, create current and voltage fluctuations<sup>†</sup>. The excess noise of an amplifier is generally characterized by the noise factor  $F$ , which is the ratio of the available output noise (including contributions by the amplifier) to the available output noise arising from the input alone [1]. Although every stage of the amplification process

---

<sup>†</sup>The terms *shot noise* and *flicker (or 1/f) noise* are often used in referring to these fluctuations. The 1/f noise is limited to the very low frequency range of the spectrum and, for all the practical situations considered in this chapter, it makes negligible contribution to the overall noise level.

contributes to the overall noise level, it is usually the case that the preamplifier (i.e., the first stage) makes the most significant contribution, simply because the noise from this stage is amplified more than that from the following stages. In any event, since the electronic noise is independent of the readout signal, there shall be no need to analyze its various components separately; instead, it shall be treated in its entirety as one source of noise. By measuring the spectrum of noise at the differential output of the system while blocking the laser beam from reaching the detectors (see Fig. 1) one obtains an accurate picture of the total electronic noise contribution.

Another manifestation of the thermal noise is the so-called *dark current* of photodetectors. Within the bulk of the semiconductor crystal constituting a photodiode, some valence electrons are thermally excited into the conduction band, giving rise to a current similar to that generated by photo-induced electrons. Unlike Johnson noise, however, the average value of the dark current is nonzero. Fluctuations of the dark current around its average value are known as dark-current-noise. These fluctuations are very similar to the shot noise which will be described in the next section. For the purpose of analysis, dark current and its associated noise may be treated by adding an equivalent (constant) light power level to the incident power on the photodetector. We will return to this topic at the end of section 3.

**3. Shot Noise in Photodetection :** Direct detection of optical signals usually entails their conversion into electrical signals by a photodetector. Photodetection is a quantum process whereby incident photons cause the release of electrons, which then go on to produce an electric current. Unfortunately, the photons do not arrive at well-defined instants of time; rather, their arrival times are random. The random arrival of photons at the detector creates fluctuations in the resulting photocurrent, which is generally known as the shot noise [2]. In this section we study properties of the shot noise as caused by coherent light. The basic property of coherent light is that the number of photons arriving during any time interval, say  $[t, t + \tau]$ , is independent of the number arriving during any other (non-overlapping) interval. If the interval is sufficiently short, then there is either one photon arriving in that interval or there is none at all. Assuming that the incident beam is monochromatic with frequency  $\nu$ , and that its power at time  $t$  is  $P_0(t)$ , the probability of a single photon arriving during the short interval  $\Delta t$  is given by

$$p\left\{n = 1, [t, t + \Delta t]\right\} = \frac{P_0(t) \Delta t}{h\nu}, \quad (2)$$

where  $h\nu$  is the energy of individual photons of frequency  $\nu$ . Not every photon of course creates one photoelectron. The quantum efficiency  $\eta$  of a photodetector is defined as the probability of a free electron being generated by an incident photon. Thus the chance that one photoelectron is released during the short interval  $\Delta t$  is given by

$$p\left\{n = 1, [t, t + \Delta t]\right\} = (\eta/h\nu) P_0(t) \Delta t. \quad (3)$$

Next we derive an expression for the probability that a number  $n$  of photoelectrons is produced in the interval  $[0, t]$  by the incident laser power  $P_0(t)$ . The probability of having  $n + 1$  electrons in  $[0, t + \Delta t]$  is related to the course of events in  $[0, t]$  by the fact that either there are  $n$  electrons in  $[0, t]$ , in which case the extra electron is created in  $[t, t + \Delta t]$ , or there are  $n + 1$  electrons in  $[0, t]$  and none in  $[t, t + \Delta t]$ . (Since  $\Delta t$  is assumed very short, the chance of two or more photoelectrons being generated in

$[t, t + \Delta t]$  is ignored.) From Eq. (3) we know the probability for the generation of one electron in a short interval; the probability of having no electrons at all in the same interval is 1 minus the probability of having one electron. Combining these arguments, we arrive at the following equation :

$$\begin{aligned} p\left\{n+1, [0, t+\Delta t]\right\} &= p\left\{n, [0, t]\right\} p\left\{1, [t, t+\Delta t]\right\} + p\left\{n+1, [0, t]\right\} p\left\{0, [t, t+\Delta t]\right\} \\ &= p\left\{n, [0, t]\right\} (\eta/h\nu) P_0(t) \Delta t + p\left\{n+1, [0, t]\right\} \left[1 - (\eta/h\nu) P_0(t) \Delta t\right], \end{aligned}$$

which, after some rearrangements, yields :

$$\frac{d}{dt} p\left\{n+1, [0, t]\right\} = (\eta/h\nu) P_0(t) \left\{p\left\{n, [0, t]\right\} - p\left\{n+1, [0, t]\right\}\right\}. \quad (4)$$

When there are no electrons in the entire interval, Eq. (4) simplifies to

$$\frac{d}{dt} p\left\{n=0, [0, t]\right\} = -(\eta/h\nu) P_0(t) p\left\{n=0, [0, t]\right\} \quad (5)$$

whose solution is readily obtained as follows :

$$p\left\{n=0, [0, t]\right\} = A \exp\left\{- (\eta/h\nu) \int_0^t P_0(t) dt\right\}.$$

The integration constant  $A$  must be equal to 1, since at  $t=0$  the probability of having no electrons must be unity. Therefore,

$$p\left\{n=0, [0, t]\right\} = \exp(-\Lambda) \quad (6)$$

where



$$\Lambda = (\eta/h\nu) \int_0^t P_0(t) dt \quad (7)$$

We now replace Eq. (6) in Eq. (4) and calculate  $p\{n = 1, [0, t]\}$ . Afterwards we calculate the probability for  $n = 2$ , then for  $n = 3$ , and so on. The general solution is found to be

$$p\{n, [0, t]\} = \exp(-\Lambda) \frac{\Lambda^n}{n!} \quad (8)^\dagger$$

Several important properties of the shot noise may be derived from the above distribution function.

For instance, the average number of photoelectrons generated in  $[0, t]$  is

$$\langle n \rangle = \sum_{n=0}^{\infty} n p\{n, [0, t]\} = \Lambda \exp(-\Lambda) \sum_{n=0}^{\infty} \frac{\Lambda^n}{n!} = \Lambda$$

That is,

$$\boxed{\langle n \rangle = (\eta/h\nu) \int_0^t P_0(t) dt} \quad (9)$$

Thus the average number of electrons released in  $[0, t]$  is proportional to the total optical energy collected in that time interval. Similarly, the variance of the number of electrons is

$$\begin{aligned} \sigma_n^2 &= \langle n^2 \rangle - \langle n \rangle^2 = \sum_{n=0}^{\infty} n^2 p\{n, [0, t]\} - \langle n \rangle^2 = \sum_{n=0}^{\infty} n^2 \frac{\Lambda^n}{n!} \exp(-\Lambda) - \Lambda^2 \\ &= \exp(-\Lambda) \sum_{n=0}^{\infty} \frac{n \Lambda^n}{(n-1)!} - \Lambda^2 = \exp(-\Lambda) \left[ \Lambda \sum_{n=0}^{\infty} \frac{\Lambda^n}{n!} + \Lambda^2 \sum_{n=0}^{\infty} \frac{\Lambda^n}{n!} \right] - \Lambda^2 = \Lambda \end{aligned}$$

---

† The probability distribution in Eq. (8) is known as the *Poisson distribution*.

The standard deviation  $\sigma_n$  of the number of photoelectrons released in  $[0, t]$  is thus given by

$$\sigma_n = \sqrt{(\eta/h\nu) \int_0^t P_0(t) dt} \quad (10)$$

Equations (9) and (10) are very important in the analysis of shot noise insofar as they relate the incident laser power  $P_0(t)$  to the strength of the photocurrent signal and the inherent shot noise which accompanies it.

The sensitivity  $\eta_s$  of a photodiode is generally defined as the average photocurrent (in Amperes) produced for 1 Watt of incident power. From Eq. (9),

$$\eta_s = \frac{\eta e}{h\nu} \quad (11)$$

where  $e = 1.6 \times 10^{-19}$  Coulomb is the electronic charge,  $h = 6.62 \times 10^{-34}$  erg. sec is Planck's constant, and  $\nu$  is the frequency of the incident light. For a typical value of  $\eta = 0.85$  at  $\lambda = 800$  nm, the photodiode sensitivity is found from Eq. (11) to be  $\eta_s = 0.55$  A/W. Now, if the signal  $S$  and the noise  $N$  are defined in terms of the integrated current (instead of the integrated number of electrons), and if the detector sensitivity  $\eta_s$  is used in place of the quantum efficiency  $\eta$ , we find

$$S = e \langle n \rangle = \eta_s \int_0^t P_0(t) dt \quad (12)$$

$$N = e \sigma_n = \sqrt{e \eta_s \int_0^t P_0(t) dt} \quad (13)$$

---

**Example 1 :** Let a 1 mW, 100 ns pulse of laser ( $\lambda = 800$  nm) be incident on a photodiode with quantum efficiency  $\eta = 0.85$ . If the pulse is uniformly integrated, the ratio of signal to noise

(averaged over many repetitions of the experiment) will be :

$$\frac{S}{N} = \frac{\langle n \rangle}{\sigma_n} = \sqrt{(\eta/h\nu) \int_0^t P_0(t) dt} = 1.85 \times 10^4 = 85.34 \text{ dB.}$$

This is a healthy signal-to-noise ratio for most practical applications.

**Spectral Analysis of Shot Noise :** Another characteristic of the shot noise is its power spectrum, which we are about to describe. Let each photoelectron generated within the detector give rise to an output electric current or voltage waveform  $h(t)^\dagger$ . The collective output  $\psi(t)$  is thus written as

$$\psi(t) = \sum_i eh(t - t_i), \quad (14)$$

where  $e$  is the electronic charge and  $t_i$  is the instant of time at which the  $i$ 'th electron has been released. Let us confine attention temporarily to that part of  $\psi(t)$  which belongs to the finite time interval  $[-T, T]$ ; later,  $T$  will be allowed to approach infinity in order to eliminate the consequences of this truncation. The Fourier transform of the truncated  $\psi(t)$  is given by

$$\begin{aligned} \Psi_T(f) &= \int_{-T}^T \psi(t) \exp(-i2\pi ft) dt = e \sum_i \exp(-i2\pi ft_i) \int_{-\infty}^{\infty} h(t) \exp(-i2\pi ft) dt \\ &= e H(f) \sum_i \exp(-i2\pi ft_i). \end{aligned} \quad (15)$$

<sup>†</sup> Quite generally,  $h(t)$  may describe the response of a cascade of elements from the detector itself to amplifiers, to filters, to signal processing circuitry, so long as all these elements are linear.

$H(f)$  is the Fourier transform of  $h(t)$ , which is usually referred to as the detection system's transfer function. The power spectral density of  $\psi(t)$  is defined as

$$S_{\psi}(f) = \lim_{T \rightarrow \infty} \left\langle \frac{1}{2T} |\Psi_T(f)|^2 \right\rangle, \quad (16)$$

where the brackets signify statistical averaging over all possible output functions  $\psi(t)$ . In Eq. (16) the normalization by  $2T$  ensures that the integral of the spectral density function  $S_{\psi}(f)$  over the entire range of frequencies remains finite. Now, replacing for  $\Psi_T(f)$  from Eq. (15) into Eq. (16) yields

$$S_{\psi}(f) = e^2 |H(f)|^2 \lim_{T \rightarrow \infty} \left\langle \frac{1}{2T} \sum_i \sum_j \exp[-i2\pi f(t_i - t_j)] \right\rangle. \quad (17)$$

Separating the terms with  $i = j$  from those with  $i \neq j$ , Eq. (17) is rewritten as

$$S_{\psi}(f) = e^2 |H(f)|^2 \lim_{T \rightarrow \infty} \left\{ \left\langle \frac{1}{2T} \sum_i 1 \right\rangle + \left\langle \frac{1}{2T} \sum_i \sum_{\substack{j \\ i \neq j}} \exp[-i2\pi f(t_i - t_j)] \right\rangle \right\}. \quad (18)$$

The first bracketed term on the right-hand-side of the above equation is the average number of photoelectrons released in  $[-T, T]$ . As for the second term, it may be decomposed and expressed as the product of terms containing  $i$  and  $j$  only, since different electrons are released independently.

Thus

$$S_{\psi}(f) = e^2 |H(f)|^2 \lim_{T \rightarrow \infty} \left\{ \frac{1}{2T} \langle n \rangle + \frac{1}{2T} \langle n(n-1) \rangle \left| \frac{\int_{-T}^T P_0(t) \exp(-i2\pi f t) dt}{\int_{-T}^T P_0(t) dt} \right|^2 \right\}. \quad (19)$$

Replacing for  $\langle n \rangle$  and  $\langle n^2 \rangle$  from Eqs. (9) and (10), we obtain

$$S_{\psi}(f) = |H(f)|^2 \lim_{T \rightarrow \infty} \left\{ \frac{e\eta_s}{2T} \int_{-T}^T P_0(t) dt + \frac{\eta_s^2}{2T} \left| \int_{-T}^T P_0(t) \exp(-i2\pi ft) dt \right|^2 \right\} \quad (20)$$

Equation (20) is the main result of this section and contains several important pieces of information. First, it shows that the transfer function of the system,  $|H(f)|^2$ , simply multiplies the total spectrum. Second, the shot noise spectral density (first term on the right-hand-side) is independent of frequency, but proportional to the average incident power. Third, the spectrum of the optical signal  $P_0(t)$ , aside from the addition of the shot noise and multiplication by  $|H(f)|^2$ , is fully reproduced within the spectrum of the signal  $\psi(t)$ .

The power spectral density of the shot noise is flat (i.e., frequency-independent) and is given by

$$N_{shot}(f) = e\eta_s \langle P_0(t) \rangle. \quad (21)$$

In Eq. (21) the brackets are used to indicate time-averaging (as opposed to ensemble averaging).

Assuming that the overall gain is unity, the system's bandwidth  $B$  may be defined as follows :

$$B = \frac{1}{2} \int_{-\infty}^{\infty} |H(f)|^2 df. \quad (22)$$

The factor 1/2 in this equation is due to  $H(f)$  having both positive and negative frequency components. The total (integrated) shot noise power within a given bandwidth then becomes

$$\langle i_{shot}^2 \rangle = \int_{-B}^B N_{shot}(f) df = 2e\eta_s \langle P_0(t) \rangle B. \quad (23)$$

The total signal power is the integral of its spectral density over the entire frequency range. Assuming that the system transfer function  $H(f)$  does not enhance, attenuate, or otherwise modify the spectrum of  $P_o(t)$ , we write

$$\begin{aligned}
 \text{Signal Power} &= \eta_s^2 \lim_{T \rightarrow \infty} \int_{-\infty}^{\infty} \frac{1}{2T} \left| \int_{-T}^T P_o(t) \exp(-i2\pi ft) dt \right|^2 df \\
 &= \eta_s^2 \lim_{T \rightarrow \infty} \frac{1}{2T} \int_{-T}^T P_o^2(t) dt \\
 &= \eta_s^2 \langle P_o^2(t) \rangle. \tag{24}
 \end{aligned}$$

In writing the second equality above we have invoked Parseval's theorem [2], which states that the area under the graph of the squared modulus of a given function is equal to the area under the graph of the squared modulus of the Fourier transform of that function.

Using Eqs. (23) and (24), one can now write the signal-to-shot-noise ratio as follows :

$$\boxed{\text{SNR} = 10 \log_{10} \left[ \frac{\eta_s^2 \langle P_o^2(t) \rangle}{2e\eta_s \langle P_o(t) \rangle B} \right]} \tag{25}$$

---

**Example 2 :** Equivalent noise power (ENP) for a photodetector is usually defined as the incident light power which produces a signal amplitude equal to the noise amplitude. For shot noise, the ENP can be calculated from Eq. (25) as  $2eB/\eta_s$ . Thus for a typical value of  $\eta_s = 0.5 \text{ A/W}$ , ENP for a shot-noise-limited detector is  $6.4 \times 10^{-19} \text{ W/Hz}$ .

---

**Dark-Current Noise :** As mentioned in the preceding section, dark-current noise of photodiodes is closely related to the photon shot noise. Their similarity arises from the fact that dark-current electrons, which are thermally generated, are produced randomly and independently of each other. If the bulk of the semiconductor which comprises the photodiode is kept at a constant temperature, then the rate of generation of the dark-current electrons is constant. Denoting the average dark current by  $I_d$ , the corresponding noise spectral density (in  $Amp/\sqrt{Hz}$ ) will be

$$i_{dark} = \sqrt{2eI_d} . \quad (26)$$

In practice the noises of the entire electronic circuitry (including the dark-current noise of the photodiodes) are lumped together and treated as a single component of the total system noise.

4. **The Laser Noise :** The laser light amplitude  $E$  is not constant, but varies randomly with time. Its fluctuations are rooted in the instabilities of the laser cavity which results in mode hopping and mode competition [3-5]. One can write the following expression for the amplitude of the light beam :

$$E(t) = E_0 \left[ 1 + \delta_e(t) \right] \exp(-i\omega t) \quad (27)$$

where  $\delta_e(t)$  is a dimensionless, complex quantity with  $|\delta_e(t)| \ll 1$  for all times  $t$ . Figure 2 is a diagram showing  $1 + \delta_e(t)$  as the sum of two vectors in the complex plane. Assuming that the complex phase of  $\delta_e(t)$  can assume all values between 0 and  $2\pi$ , it is observed that  $1 + \delta_e(t)$  is confined to a small disk centered at (1,0) in the complex plane.

The laser power is proportional to the electric field intensity and is therefore given by :

$$P(t) \propto |E_0|^2 \left[ 1 + \delta_e(t) + \delta_e^*(t) + |\delta_e(t)|^2 \right] \simeq P_0 \left\{ 1 + 2 \operatorname{Real} [\delta_e(t)] \right\}. \quad (28)$$

The rms fluctuations of the laser power are thus equal to  $2P_0\Delta_e$  where

$$\Delta_e = \sqrt{\langle \operatorname{Real}^2 [\delta_e(t)] \rangle}. \quad (29)$$

Unlike the spectra of shot noise and Johnson noise, the spectrum of  $\delta_e(t)$  is not necessarily flat. In general, the frequency response of any measurement system has a finite range and a nonuniform magnitude, thus requiring that the spectral content of  $\delta_e(t)$  be properly trimmed and adjusted, before using it in Eq. (29) to calculate the rms noise value.

When one measures the spectrum of the laser power fluctuations using a photodetector (i.e., intensity detection), one obtains a trace on the spectrum analyzer which, in addition to the desired spectrum, contains contributions from the shot noise and the thermal noise of the detection circuitry. The thermal noise, however, may be measured independently by observing the detector output when the beam is blocked, and the shot noise may be estimated from Eq. (23) using the average incident



light power  $P_0$ . It may also happen that the fluctuations of  $\delta_e(t)$  have a limited frequency content, in which case the noise outside the range of frequencies of  $\delta_e(t)$  is identified as the sum of shot noise and electronic noise. Since both the shot and thermal noises have flat spectra, one can then proceed to subtract their contributions from the total spectrum and obtain the spectrum of the laser power fluctuations<sup>†</sup>.

---

**Example 3:** Figure 3 shows the measured noise spectra at the output of the laser monitor in a typical experiment (see Fig. 1). The lower trace corresponds to the electronic noise which is monitored in the absence of the light beam, and the upper trace shows the total noise with an incident light power of  $P_0 = 380 \mu W$ . The PIN photodiode/amplifier used for these measurements had a sensitivity of  $\eta_s = 0.42 A/W$  at the laser wavelength of 680 nm, and a gain (i.e., current to voltage conversion factor) of  $G = 10^4 V/A$ . The electronic noise level read from Fig. 3 is -84 dBm. This is the power delivered to a  $50 \Omega$  resistor in a bandwidth of 30 kHz; thus the rms thermal noise voltage at the amplifier output is  $v_{th} = 80 nV/\sqrt{Hz}$ , and the corresponding noise current at the output of the photodiode prior to amplification is  $i_{th} = 8 pA/\sqrt{Hz}$ . The shot noise current density is calculated from Eq. (23) as follows :

$$i_{sh} = \sqrt{2e \eta_s P_0} = \sqrt{2 \times 1.6 \times 10^{-19} \times 0.42 \times 380 \times 10^{-6}} = 7.2 pA/\sqrt{Hz}.$$

Since the total noise power in Fig. 3 is about 14 dB (i.e., a factor of 25) above the thermal noise level, we have

$$\frac{i_{th}^2 + i_{sh}^2 + i_{laser}^2}{i_{th}^2} = 25,$$

---

<sup>†</sup>Since the shot noise spectral level is proportional to  $P_0$ , whereas that of the laser power fluctuations is proportional to  $P_0^2$ , it is tempting to suggest that a plot of the total noise power versus  $P_0$  should behave as  $a + bP_0 + cP_0^2$ , from which one can sort out the individual contributions. The problem with this approach, however, is that  $\delta_e(t)$  itself may depend in an unknown manner on  $P_0$ , causing the argument to fail.

from which we find  $i_{laser} = 38.5 \text{ pA}/\sqrt{\text{Hz}}$ . This is the rms current fluctuation caused by the laser noise at the photodiode output (prior to amplification). The laser noise may be normalized by the average laser power and stated as a relative intensity noise (RIN), that is,

$$\text{RIN} = 20 \log (i_{laser} / \eta_s P_0) = 20 \log \frac{38.5 \times 10^{-12}}{0.42 \times 380 \times 10^{-6}} \approx -132.5 \text{ dB}.$$

Since the laser noise spectrum in Fig. 3 is relatively flat through the frequency range  $f = 0$  to  $f = 10$  MHz, one can easily integrate the RIN over the entire 10 MHz bandwidth of the system and obtain the figure of -62.5 dB for the integrated RIN. Comparison with Eqs. (28) and (29) then shows that the rms value of  $\text{Real} [\delta_e(t)]$ , confined to a 10 MHz bandwidth, is  $\Delta_e \approx 4 \times 10^{-4}$ .

---

**Example 4 :** The spectra shown in Fig. 4 correspond to the output of a laser monitor which is a low-noise, hybrid PIN photodiode/amplifier with a sensitivity of  $\eta_s = 0.5 \text{ A/W}$  at  $\lambda = 830 \text{ nm}$  [7]. The detector's current to voltage conversion factor is  $G = 3.64 \times 10^4 \text{ V/A}$ . The lower trace shows the spectrum of the detector output in the absence of light. The -88 dBm electronic noise level corresponds to  $v_{th} = 51 \text{ nV}/\sqrt{\text{Hz}}$  at the amplifier output and to  $i_{th} = 1.4 \text{ pA}/\sqrt{\text{Hz}}$  at its input. The upper trace was obtained when  $39 \text{ }\mu\text{W}$  of laser light was incident on the detector. From Eq. (23) the shot noise current density (prior to amplification) is found to be  $i_{sh} = 2.5 \text{ pA}/\sqrt{\text{Hz}}$ , thus

$$(i_{th}^2 + i_{sh}^2) / i_{th}^2 \approx 4.2 = 6.2 \text{ dB}.$$

Therefore, the thermal-plus-shot noise level must be about 6.2 dB above the thermal noise level in Fig. 4. The remaining noise is due to fluctuations of the laser power, which may now be separated out. Let us approximate the frequency-dependence of the total noise density in Fig. 4 with a linear function as follows :

$$10 \log \left( \frac{i_{th}^2 + i_{sh}^2 + i_{laser}^2}{i_{th}^2} \right) \approx 23 - 1.3 f \quad (f \text{ in MHz}).$$

This expression leads to the following frequency-dependence for the laser noise :

$$(i_{laser}/i_{th})^2 \simeq -4.2 + 200 \exp(-0.3 f) \quad (f \text{ in MHz}).$$

The above function is now averaged over the frequency range from  $f = 0$  to  $f = 10$  MHz, yielding the average value of 59 for  $(i_{laser}/i_{th})^2$ . Thus the average noise current arising from the laser power fluctuations (within a 10 MHz bandwidth) is  $i_{laser} \simeq 10.75 \text{ pA}/\sqrt{\text{Hz}}$ . Normalization by  $\eta_s P_0$  yields an average RIN of -125.2 dB, and the rms value of the  $E$ -field fluctuations over the 10 MHz bandwidth of interest is  $\Delta_e \simeq 8.7 \times 10^{-4}$ .

---

5. **Noise Due to Disk Surface Reflectivity Fluctuations and Depolarization :** In the following analysis it will be assumed that the disk spins at a constant speed, and that the noise is measured on an erased track, that is, one with no reverse-magnetized domains. The effective light power incident on the disk surface is denoted by  $P_0$ , and the losses due to reflections from or transmissions through the various optical elements in the system are ignored. (If need be, however, such losses can easily be incorporated into the results later.) The three sources of noise considered here include : *i*) amplitude and phase variations of the  $X$ -polarized reflected light; *ii*) random depolarization of the incident ( $X$ -polarized) beam; and *iii*) amplitude and phase fluctuations of the magneto-optically generated component of polarization along  $Y$  [8-11]. The physical mechanisms responsible for these noises are described below.

For various reasons, there will be fluctuations in the effective reflectivity  $r_x$  for the  $X$ -component of polarization. First, the material composition and/or structure varies across the disk. Second, if there are grooves on the disk surface, their edge roughness is likely to scatter the light in a random fashion. Third, there are residual amounts of off-track and defocus errors that vary with time and, therefore, cause the reflectivity to fluctuate. Some of these noise sources are fixed on the disk and, consequently, their time-dependencies scale with the disk velocity; others, such as those due to mechanical vibrations or focus/track errors, are caused by fluctuations elsewhere in the system and do not scale with the velocity. In any event, assuming that these fluctuations are small, one writes :

$$r_x(t) = r_{x0} [1 + \delta_x(t)]; \quad |\delta_x| \ll 1 \quad (30)$$

where  $\delta_x(t)$  is a small, dimensionless, complex coefficient, representing the fractional variations of  $r_x$ .

There **exists** the possibility of conversion of some of the  $X$ -polarized incident light into  $Y$ -polarized reflected light due to depolarization, as distinct from the magneto-optic conversion. This phenomenon is partly due to substrate-birefringence, but is also caused by the various scattering mechanisms at work on the disk surface. Perhaps the best way to characterize the depolarization contribution to noise is by defining a disk reflection coefficient  $r_{xy}$  as follows :

$$r_{xy}(t) = r_{xo} \delta_{xy}(t); \quad |\delta_{xy}| \ll 1 \quad (31)$$

where, as before,  $\delta_{xy}(t)$  is a small, dimensionless, complex coefficient.

Finally, there is the magneto-optic contribution to the  $Y$ -polarized reflected light. For a completely erased track, one may write the  $Y$ -component of the reflectivity as follows :

$$r_y(t) = r_{yo} [1 + \delta_y(t)]; \quad |\delta_y| \ll 1. \quad (32)$$

Some of the fluctuations in  $r_y$  originate from the structural/magnetic variations of the disk material along the length of the track, but there is also a correlation between fluctuations in  $r_y$  and those in  $r_x$ . For instance, if more  $X$ -polarized light is reflected, then less light will be available to interact with the magnetization of the material and produce the  $Y$ -polarized component. For the sake of simplicity, we shall ignore all possible correlations among  $\delta_x$ ,  $\delta_{xy}$ , and  $\delta_y$ , and treat these parameters as independent random variables.

The phase compensator in the data detection branch of the readout system of Fig. 1 eliminates the nominal ellipticity of the beam by bringing  $r_{xo}$  and  $r_{yo}$  in phase with each other. Consequently, we assume at the outset that  $r_{yo}/r_{xo}$  is real and, to emphasize its realness, we shall write it as  $|r_{yo}/r_{xo}|$ . The compensator will have no influence whatsoever on the noise coefficients  $\delta_x$  and  $\delta_y$ , and will modify  $\delta_{xy}$  only by the addition of an irrelevant constant phase angle. The power incident on individual detectors is thus written as :

$$P_1, P_2 \propto \left| \frac{E_0}{\sqrt{2}} (1 + \delta_e) [\gamma r_{xo} (1 + \delta_x) \pm r_{xo} \delta_{xy} \pm r_{yo} (1 + \delta_y)] \right|^2$$

where the plus (minus) sign applies to the incident power  $P_1$  ( $P_2$ ) on detector #1 (#2). Expanding the above expression and ignoring the second order terms in the noise variables, we find the photocurrents  $S_1$  and  $S_2$  of the detectors as follows :

$$S_1, S_2 \approx \frac{1}{2} \eta_s P_0 \left[ \gamma |r_{xo}| \pm |r_{yo}| \right]^2 + \eta_s P_0 |r_{xo}|^2 \left[ \gamma \pm \left| \frac{r_{yo}}{r_{xo}} \right| \right] \text{Real} \left[ \gamma(\delta_e + \delta_x) \pm \delta_{xy} \pm \left| \frac{r_{yo}}{r_{xo}} \right| (\delta_e + \delta_y) \right] \quad (33)$$

The sum of the two detector signals is thus given by

$$S_1 + S_2 \approx \eta_s P_0 \gamma^2 |r_{xo}|^2 \left[ 1 + |r_{yo}/\gamma r_{xo}|^2 \right] + 2\eta_s P_0 |r_{xo}|^2 \left\{ \gamma^2 \text{Real} [\delta_e + \delta_x] + \left| \frac{r_{yo}}{r_{xo}} \right| \text{Real} [\delta_{xy}] + \left| \frac{r_{yo}}{r_{xo}} \right|^2 \text{Real} [\delta_e + \delta_y] \right\} \quad (34)$$

The first term on the right-hand-side of Eq. (34) is the average photocurrent signal of the two detectors. The second term represents the fluctuations of this signal, and consists of three contributions: The contributions due to the laser noise  $\delta_e$  and the noise in the  $X$ -component of reflectivity  $\delta_x$  are proportional to  $\gamma^2$ . The second contribution comes from depolarization noise  $\delta_{xy}$  and is proportional to  $|r_{yo}/r_{xo}|$ . Note that individual channels have a much larger noise component arising from depolarization, but in adding the two channels, much of this noise cancels out. The third contribution is a combination of the laser noise  $\delta_e$  and the noise in the magneto-optic component of the reflected light  $\delta_y$ ; it is proportional to  $|r_{yo}/r_{xo}|^2$ . In practice,  $|r_{yo}/r_{xo}|$  is usually much smaller than  $\gamma^2$  and, therefore, the second and third contributions to the noise may be neglected. Under these circumstances the total fluctuations of the sum signal arise from electronic noise, shot noise, laser noise, and the  $r_x$  noise. Since all but the last of these fluctuations can be measured when the disk is stopped, the excess noise observed upon spinning the disk is attributed to the  $r_x$  contribution.

The output of the differential detection system is proportional to the difference of the two detector signals, namely,

$$S_1 - S_2 \approx 2\eta_s P_0 \gamma |r_{xo}| |r_{yo}| \left\{ 1 + \text{Real} [2\delta_e + \delta_x + \delta_y] + \left| \frac{r_{yo}}{r_{xo}} \right| \text{Real} [\delta_{xy}] \right\} \quad (35)$$

The first term on the right-hand-side of this equation is the magneto-optic signal, observed in the erased state of the disk. The second term is the combined contribution of the laser noise  $\delta_e$  and the reflectivity noises  $\delta_x$  and  $\delta_y$ ; depolarization noise  $\delta_{xy}$  constitutes the third term. Note that the depolarization term has a larger coefficient than the other noise term, and may therefore be the dominant noise in magneto-optical readout.

One observes that in going from the sum signal of Eq. (34) to the difference signal of Eq. (35), the contribution of  $(\delta_e + \delta_x)$  is attenuated by a factor of  $|r_{yo}/\gamma r_{xo}|$ . The reason is that the laser noise and the  $r_x$  noise are identical in the two channels and, for a balanced system, they cancel out. The residual noise observed in this instance is due to the interference with the magneto-optic component,  $r_{yo}$ . The same thing, of course, happens to the  $r_y$  noise, but there the interference with  $r_x$  creates a term larger than the original  $r_y$  noise; that is why the coefficient of  $(\delta_e + \delta_y)$  in the difference signal is larger than that in the sum signal by a factor of  $|\gamma r_{xo}/r_{yo}|$ . Similar considerations apply to the depolarization noise  $\delta_{xy}$ .

The signals  $S_1$  and  $S_2$  of the individual detectors may themselves be written in terms of the sum and difference signals in the following way :

$$S_1, S_2 = \frac{1}{2} (S_1 + S_2) \pm \frac{1}{2} (S_1 - S_2) \quad (36)$$

It thus becomes clear that the sum signal is the common-mode signal, shared by the two detectors and rejected only by the differential amplifier. Practical differential amplifiers, unfortunately, have a finite common-mode-rejection-ratio (CMRR), and the noise accompanying the sum signal in Eq. (34) also appears at the output, albeit after a substantial attenuation. In the remainder of this section we shall assume that the differential amplifier has a large CMRR, and thus proceed to ignore the common-mode noise.

The rms values of the various fluctuating parameters (within the bandwidth of the system) are now defined as follows :

$$\Delta_x = \sqrt{\langle \text{Real}^2 [\delta_x(t)] \rangle} \quad (37a)$$

$$\Delta_y = \sqrt{\langle \text{Real}^2 [\delta_y(t)] \rangle} \quad (37b)$$

$$\Delta_{xy} = \sqrt{\langle \text{Real}^2 [\delta_{xy}(t)] \rangle} \quad (37c)$$

The total signal and the rms noise (including thermal and shot noises but excluding the residual common-mode noise) at the differential output are thus written as

$$i_{\text{signal}} \approx 2 \eta_s P_0 \gamma |r_{x0}| |r_{y0}| \quad (38)$$

$$i_{\text{noise}}^2 \approx \left\{ 2i_{th}^2 + 2e \eta_s P_0 \gamma^2 |r_{x0}|^2 \left[ 1 + |r_{y0}/\gamma r_{x0}|^2 \right] \right\} B \\ + \left( 2\eta_s P_0 \gamma |r_{x0}| |r_{y0}| \right)^2 \left( 4\Delta_e^2 + \Delta_x^2 + \Delta_y^2 + |r_{x0}/r_{y0}|^2 \Delta_{xy}^2 \right) \quad (39)$$

From a practical system design standpoint, there is an advantage in choosing  $\gamma$  as small as possible, so that the most light can get through to the disk during the writing process. However, Eqs. (38) and (39) indicate that  $\gamma$  cannot be made too small either, since in that eventuality the thermal noise becomes dominant and the overall signal-to-noise ratio (SNR) suffers.  $\gamma$  must therefore be large enough to bring the total noise level well above the level of the thermal noise. In the ideal case, when  $\gamma$  is sufficiently large to make the thermal noise negligible, the SNR becomes independent of  $\gamma$  and can be expressed as follows :

$$SNR_{\text{ideal}} \approx \frac{2\eta_s P_0 |r_{y0}|^2}{eB \left[ 1 + |r_{y0}/\gamma r_{x0}|^2 \right] + 2\eta_s P_0 |r_{y0}|^2 \left[ 4\Delta_e^2 + \Delta_x^2 + \Delta_y^2 + |r_{x0}/r_{y0}|^2 \Delta_{xy}^2 \right]} \quad (40)$$



Of course, the ideal SNR is never attained in practice, but it can be approached closely. From Eq. (39) the critical value  $\gamma_c$  of  $\gamma$ , at which the thermal noise strength equals the combined strength of all the other noises, is given by

$$\gamma_c^2 = \frac{i_{th}^2}{e \eta_s P_0 |r_{xo}|^2 \left\{ 1 + |r_{yo}/\gamma r_{xo}|^2 + 2 (\eta_s/eB) P_0 |r_{yo}|^2 \left[ 4\Delta_e^2 + \Delta_x^2 + \Delta_y^2 + |r_{xo}/r_{yo}|^2 \Delta_{xy}^2 \right] \right\}} \quad (41)$$

When  $\gamma = \gamma_c$ , the SNR is only 3 dB below its ideal value; when  $\gamma = 2\gamma_c$ , the gap shrinks to 1 dB, and with  $\gamma = 3\gamma_c$ , the ideal SNR is only 0.5 dB away. Further increases of  $\gamma$  beyond these values are hardly justified; in fact, for large values of  $\gamma$ , the common-mode noise begins to appear in the differential output, causing the SNR to deteriorate.

According to Eq. (40), beyond the shot noise limit one is in a regime where the dominant noise is proportional to the signal; therefore, increasing the laser power  $P_0$  does not enhance the SNR. In this regime, if the depolarization noise  $\delta_{xy}$  happens to be an important contributor, then increasing  $r_{yo}$  will diminish the noise. On the other hand, if the laser noise  $\delta_e$  and/or the reflectivity noises  $\delta_x$  and  $\delta_y$  are dominant, increases in  $r_{yo}$  will have no effect on the SNR. These are some of the issues to contemplate in optimizing the readout system.

---

**Example 5 :** Consider the readout system of Fig. 1, operating under the following conditions : laser wavelength  $\lambda = 680$  nm, effective laser power incident on the disk  $P_0 = 2$  mW, disk reflectivity  $r_x = 0.5$ , disk magneto-optic reflection coefficient  $r_y = 0.005$ , leakage parameter of the beam-splitter  $\gamma = 0.4$ , photodetector sensitivity  $\eta_s = 0.42$  A/W, preamplifier conversion factor  $G = 3.3 \times 10^4$  V/A, and differential amplifier's gain = 13. The laser noise for this system was analyzed in Example 3, and the rms fluctuations of the  $E$ -field were found to be  $\Delta_e \simeq 4 \times 10^{-4}$ .

Figure 5(a) shows the spectra of the differential amplifier's output voltage, measured with the light blocked from both detectors (lower trace), and with the light reaching the detectors while the disk was stopped (upper trace). The electronic noise level at -65 dBm is the sum of contributions

from the two detectors and the differential amplifier. Referred to individual photodiode currents (prior to amplification), this thermal noise has a density of  $i_{th} \approx 1.2 \text{ pA}/\sqrt{\text{Hz}}$ . The shot noise current density for the  $40 \text{ }\mu\text{W}$  of incident power on each photodiode is calculated as  $i_{sh} \approx 2.3 \text{ pA}/\sqrt{\text{Hz}}$ . This means that the thermal-plus-shot noise level is about 6.7 dB above the thermal noise, as is indeed the case in Fig. 5(a). Apparently, the laser noise does not contribute much to the upper trace in Fig. 5(a), in agreement with Eq. (39) which predicts a laser noise current density of  $0.4 \text{ pA}/\sqrt{\text{Hz}}$  at the output of the differential amplifier. (The common-mode contribution of the laser noise, estimated from Eq. (34), is also negligible. Assuming the reasonable value of  $\text{CMRR} = 100$ , the common-mode laser noise appearing at the differential output is only about  $0.04 \text{ pA}/\sqrt{\text{Hz}}$ .)

Figure 5(b) shows two spectra of the differential amplifier's output with the disk spinning. The lower trace corresponds to an erased track, while the upper trace contains a recorded 8 MHz carrier signal. The erased track is about as noisy as the recorded one, leading one to believe that jitter and other signal fluctuations do not contribute much to the noise. Integrating the erased-state noise over the frequency range from  $f = 0$  to  $f = 10 \text{ MHz}$ , we obtain the figure of  $-30 \text{ dBm}$ . This is the total noise power delivered to a  $50 \text{ }\Omega$  resistor at the amplifier's output, and corresponds to an rms noise voltage of  $7 \text{ mV}$ . Dividing by the net gain of the system, the equivalent rms noise current is found to be  $16.3 \text{ nA}$ . After subtracting the contributions from thermal and shot noises, we find the remaining rms noise to be  $11.5 \text{ nA}$  which, according to Eq. (39), can arise from a small amount of depolarization noise ( $\Delta_{xy} \approx 0.7 \times 10^{-4}$ ). Of course, reflectivity fluctuations could as well be responsible for the observed noise, but the necessary values of  $\Delta_x$  or  $\Delta_y$  must be larger than  $\Delta_{xy}$  by a factor of  $|r_{xo}/r_{yo}| = 100$ .

Finally, Fig. 5(c) shows the spectrum of the differential output with one of the two detectors blocked. Although the erased-track spectrum is not shown here, it is reasonable to neglect the noise associated with the signal (i.e., jitter and signal amplitude fluctuation noise). The integrated noise power within the  $10 \text{ MHz}$  bandwidth of the system is  $-30 \text{ dBm}$ , corresponding to a preamplification rms noise current of  $16.3 \text{ nA}$ . Subtracting the thermal noise (of two detectors) and the shot noise (of one detector) from this figure, we find the remaining noise current to be  $13.6 \text{ nA}$ . According to Eq. (33), this noise is almost exclusively due to laser power fluctuations, thus ruling out the possibility

of a large  $r_x$  noise. One concludes, therefore, that the differential output noise (with neither detector blocked) is due either to a small  $\Delta_{xy}$  or a large  $\Delta_y$ , but not a large  $\Delta_x$ .

---

**Example 6 :** Consider the readout system of Fig. 1, operating under the following conditions : laser wavelength  $\lambda = 830$  nm, effective laser power incident on the disk  $P_0 = 2$  mW, disk reflectivity  $r_x = 0.4$ , disk magneto-optic reflection coefficient  $r_y = 0.004$ , leakage parameter of the beam-splitter  $\gamma = 0.35$ , photodetector sensitivity  $\eta_s = 0.5$  A/W, preamplifier conversion factor  $G = 3.3 \times 10^4$  V/A, and differential amplifier gain = 18. The laser noise for this system was analyzed in Example 4, and the rms fluctuations of the  $E$ -field were found to be  $\Delta_e \simeq 8.7 \times 10^{-4}$ .

Figure 6 shows the measured spectra of the differential amplifier's output voltage under various circumstances. With the light blocked from both detectors the electronic noise level is at -62 dBm (lower trace in Fig. 6(a)). Referred to individual photodiode currents (prior to amplification), this thermal noise has a density of  $i_{th} \simeq 1.2$  pA/ $\sqrt{\text{Hz}}$ . The shot noise current density for the 20  $\mu\text{W}$  of incident power on each photodiode is calculated as  $i_{sh} \simeq 1.8$  pA/ $\sqrt{\text{Hz}}$ . This means that the thermal-plus-shot noise level is about 5 dB above the thermal noise. (See the middle trace in Fig. 6(a) which shows the output noise spectrum with light reaching both detectors while the disk is stopped.) The laser noise contributes only 0.5 dB in this case since, according to Eq. (39), its current density is 0.6 pA/ $\sqrt{\text{Hz}}$ . (The common-mode contribution of the laser noise, estimated from Eq. (34), is negligible : if CMRR = 100, the common-mode laser noise at the differential output is only about 0.1 pA/ $\sqrt{\text{Hz}}$ .)

The upper trace in Fig. 6(a) shows the spectrum of the differential output with the disk spinning and the track containing a 4 MHz carrier signal. Assuming the erased track has the same level of noise as the recorded one (i.e., ignoring jitter noise and other signal fluctuations) we integrate the noise from  $f = 0$  to  $f = 10$  MHz and obtain the figure of -27 dBm. This is the noise power delivered to a 50  $\Omega$  resistor at the amplifier's output, and corresponds to an rms noise voltage of 10 mV. Dividing by the net gain of the system, the equivalent rms noise current is found to be 16.8 nA. After subtracting the contributions of the thermal noise and the shot noise, we find the remaining rms noise to be 13.7 nA which, according to Eq. (39), can arise from a small amount of depolarization

noise ( $\Delta_{xy} \simeq 1.2 \times 10^{-4}$ ). Of course, reflectivity fluctuations could as well be responsible for the observed noise, but the necessary values of  $\Delta_x$  or  $\Delta_y$  must be larger than  $\Delta_{xy}$  by a factor of  $|r_{xo}/r_{yo}| = 100$ .

Figure 6(b) shows the spectrum of the differential output with one of the two detectors blocked. Again, the erased-track spectrum is not shown here, but it is reasonable to neglect the noise associated with the signal. The integrated noise power within the 10 MHz bandwidth of the system is -24 dBm, corresponding to a preamplification rms noise current of 23.7 nA. Subtracting the thermal noise (of two detectors) and the shot noise (of one detector) from this figure, we find the remaining noise current to be 22.4 nA. According to Eq. (33), this noise arises from laser power fluctuations  $\Delta_e$ , reflectivity fluctuations  $\Delta_x$ , and depolarization  $\Delta_{xy}$ . Using the known values of  $\Delta_e$  and  $\Delta_{xy}$  in Eq. (33), we find  $\Delta_x = 6.6 \times 10^{-4}$ . One concludes, therefore, that the output noise when neither detector is blocked is due either to a small  $\Delta_{xy}$  or a large  $\Delta_y$ , but not a large  $\Delta_x$ .

---

**6. Jitter and Signal-Amplitude Fluctuations :** In this section we present computer simulation results pertaining to the noise arising from fluctuations of the information-carrying signal. Distinction will be made between jitter, which is caused by random variations of the zero-crossings of the signal waveform, and signal-amplitude-fluctuation noise. The basic waveform considered here is a 4 MHz, 50% duty-cycle carrier signal whose amplitude alternates periodically between the values of +1 and -1, transitions between the two levels of the signal being infinitely sharp. The power spectrum of this waveform was computed numerically, and the result is shown in Fig. 7. The (approximate) sampling intervals in the time and frequency domains were, respectively, 0.5 ns and 30 kHz, corresponding to a total number of samples  $N_{max} = 65536$ . The spectrum contains the first and third harmonics of the waveform at 4 MHz and 12 MHz. With the unity power of the square-wave signal corresponding to 0 dB, the fundamental and the third harmonic power levels are at -0.912 dB and -10.455 dB, respectively. In Fig. 7 the spikes at frequencies other than 4 and 12 MHz are numerical noise due to truncation errors, their very small magnitudes attesting to the basic accuracy of the numerical routine.

Next, we introduced jitter in the transition times of the signal. A random number generator selected values in the interval  $[-\Delta t, \Delta t]$  with uniform distribution. These random numbers were then added independently to individual transition times of the ideal signal, creating a waveform with jitter magnitude of  $\Delta t$ . As an example, Fig. 8 shows a section of the signal between  $t = 0$  and  $t = 2 \mu s$ , with  $\Delta t = 25$  ns of jitter. The computed power spectra of the resulting noisy signals are shown in Figs. 9(a)-(d) which correspond, respectively, to jitter magnitudes of  $\Delta t = 3, 5, 15$  and 25 ns. (The spectral power densities are computed in a 30 kHz bandwidth.) Note that within the bandwidth of interest the spectra are relatively flat and that, understandably, their levels rise with the increasing magnitude of jitter.

Effects of amplitude fluctuations on the signal waveform and its power spectrum are shown in Fig. 10. Figure 10(a) is a section of a jitter-free waveform, exhibiting random amplitude variations in its upper half; the values of these signal amplitudes were chosen randomly and independently from the interval  $[0.85, 1.00]$  with a uniform probability distribution. The corresponding power spectrum in Fig. 10(b) shows a significant noise contribution only at low frequencies. A similar conclusion is

arrived at upon inspecting the spectrum of Fig. 10(c), which corresponds to a signal whose positive amplitude fluctuates within [0.70, 1.00] and has, in addition, a jitter noise component with  $\Delta t = 3$  ns. Comparison with Fig. 9(a) clearly indicates that the high frequency noise is solely due to jitter, whereas at low frequencies the noise may be attributed to the amplitude fluctuations.

Finally, Fig. 11(a) shows a section of a signal waveform with positive amplitude fluctuations within [0.70, 1.00], negative amplitude fluctuations within [-1.00, -0.70], and jitter magnitude of  $\Delta t = 3$  ns. The corresponding spectrum in Fig. 11(b) shares its general features with that in Fig. 10(c), but it has a larger noise content in the low frequency regime which is, of course, expected. The spectrum in Fig. 11(c) is obtained when the jitter magnitude is increased to  $\Delta t = 15$  ns while amplitude fluctuations are maintained at their previous level. The noise in this instance is almost exclusively due to jitter, as a comparison with Fig. 9(c) indicates.

**Effects of Finite Beam Size on Signal and Noise Spectra :** Up to this point we have ignored the fact that the focused spot on the disk surface has a finite diameter. The effects of the finite spot size are readily incorporated into the preceding results if one ignores the diffraction effects. The signal at the output of the readout system is then obtained by convolving the intensity profile of the spot with the recorded pattern of information on the disk. For the sake of simplicity let us assume a Gaussian intensity distribution for the spot as follows :

$$I(x) = \frac{1}{\sqrt{\pi\rho^2}} \exp(-x^2/\rho^2) . \quad (42)$$

Here  $x$  is the spatial coordinate on the disk surface along the track, and  $\rho$  is a measure of the spot size (FWHM =  $1.66 \rho$ ). The function in Eq. (42) is properly normalized so that the integrated spot intensity is unity. If the actual pattern of recorded data along the track is denoted by  $\psi_0(x)$ , and if  $v_0$  is the disk velocity, then the output signal will be

$$\psi(v_0 t) = \int_{-\infty}^{\infty} I(x) \psi_0(x - v_0 t) dx. \quad (43)$$

The function  $\psi(x)$ , the result of convolution between  $I(x)$  and  $\psi_0(x)$ , is scaled along the horizontal axis by the factor  $v_0$  in order to yield the time dependence of the observed signal. Upon Fourier transformation, the convolution turns into the product of the Fourier transforms of the individual functions, that is,

$$\mathcal{F}\{\psi(v_0 t)\} = v_0 \mathcal{F}\{I(v_0 t)\} \mathcal{F}\{\psi_0(v_0 t)\}. \quad (44)$$

The transform of the Gaussian function is readily calculated as follows :

$$v_0 \mathcal{F}\{I(v_0 t)\} = \exp\left\{-\left(\pi\rho/v_0\right)^2 f^2\right\}. \quad (45)$$

If the spectra of  $\psi_0(v_0 t)$  and  $\psi(v_0 t)$  are denoted by  $\mathcal{S}_{\psi_0}(f)$  and  $\mathcal{S}_{\psi}(f)$ , respectively, we will have

$$\mathcal{S}_{\psi}(f) = \exp\left\{-2\left(\pi\rho/v_0\right)^2 f^2\right\} \mathcal{S}_{\psi_0}(f) \quad (46)$$

Equation (46) shows that the spectrum of the signal (including jitter and amplitude noise) is attenuated by a multiplicative factor that is the Fourier transform of the spot intensity distribution. In the literature, this effect is usually attributed to the *Modulation Transfer Function* (MTF) of the optical readout system. The frequency at which the spectrum is attenuated by a factor of 2 is a measure of the width of the MTF. According to this definition, the width of the Gaussian function in Eq. (46) is approximately equal to  $v_0/5\rho$ .

---

**Example 7 :** In Fig. 5(b) the recorded carrier is read from the disk at the constant velocity of  $v_0 = 14 \text{ m/s}$ . Assuming a Gaussian profile for the focused spot with FWHM =  $1 \mu\text{m}$  (i.e.,

$\rho = 0.6 \mu\text{m}$ ), we find an MTF attenuation of 10 dB at  $f = 8 \text{ MHz}$ . Similarly, in Fig. 6 where  $v_0 = 10 \text{ m/s}$  and  $\rho = 0.7 \mu\text{m}$ , the attenuation of the 4 MHz carrier is found from Eq. (46) to be 6.7 dB.

---

Of the various noises discussed in the present chapter, the spectra of the electronic, shot, and laser noise are obviously unaffected by the MTF. The spectrum of the disk noise, on the other hand, is attenuated in a manner similar to that of the information signal as described by Eq. (46). An example of this phenomenon may be seen in Fig. 12, where the spectrum of an erased track is shown for three different disk velocities [12]. In each case, the tail of the trace corresponds to thermal + shot + laser noise, which is velocity-independent. The low frequency magnitudes of the spectral density functions drop by 3 dB each time the velocity is doubled. This reflects the fact that the noise power is constant; in other words, when the velocity is doubled (causing the spectrum to stretch over a range of frequencies twice as large) the magnitudes of the spectral density drop by a factor of 2 (i.e., 3 dB) in order to maintain the total (integrated) power. If one assumes that the underlying sources of disk noise have flat spectra, then the curves of Fig. 12 are simply plots of the MTF.

---

**Example 8 :** In Fig. 12 the curve corresponding to  $v_0 = 6 \text{ m/s}$  drops by about 12 dB between  $f = 0$  and  $f = 4 \text{ MHz}$ . Assuming that the curve represents the actual MTF of the system and that the MTF has the Gaussian form of Eq. (46), we find  $\rho = 0.56 \mu\text{m}$ , corresponding to  $\text{FWHM} = 0.93 \mu\text{m}$ .

---



## PROBLEMS

- 9.1) In deriving Eq. (19) from Eq. (18) several steps were left out. Describe the missing steps and fill the gaps in the derivation.
- 9.2) Photomultiplier tubes (or avalanche photodiodes) multiply photo-induced electrons (or electron-hole pairs) and output  $G$  electrons for every captured photon. In general,  $G$  is not the same for all photons; instead, it should be considered a random variable with average  $\langle G \rangle$  and square-average  $\langle G^2 \rangle$ . The multiplication process is rapid enough to be assumed instantaneous, and the value of  $G$  for a given photon is independent of that for any other photon. Assuming an incident laser beam with power  $P_0(t)$ , determine the spectra of signal and shot noise at the photomultiplier output.
- 9.3) Equation (33) was derived from the equation immediately preceding it, but the details of derivation were left out. Examine the approximations involved in this derivation and the conditions under which the second-order terms in  $\delta_e$ ,  $\delta_x$ ,  $\delta_y$  and  $\delta_{xy}$  may be ignored. Pay special attention to those remaining terms that contain  $r_{y0}$ , since in practice the magnitudes of  $|r_{y0}/r_{x0}|$  and  $|r_{y0}/\gamma r_{x0}|$  are likely to be comparable to  $\delta_e$ ,  $\delta_x$ , etc.
- 9.4) Obtain the first few terms in the Fourier series representation of a periodic square-wave function such as the one whose spectrum is shown in Fig. 7. Assume that the function has frequency  $f_0$  with 50% duty cycle, and that its amplitude is confined to the values of +1 and -1. Show that the first and third harmonics of the waveform have power levels of -0.912 dB and -10.455 dB, respectively, as the numerically computed spectrum in Fig. 7 indicates.
- (The numerical results are based on the following formula :

$$S_{\psi}(m) = 2 \left| \frac{1}{N_{max}} \sum_{n=0}^{N_{max}-1} \psi(n) \exp \left[ -\frac{i 2\pi mn}{N_{max}} \right] \right|^2$$

where the function  $\psi(t)$  is uniformly sampled at times  $t = n \Delta t$ , its power spectrum  $S_{\psi}(f)$  is sampled (also uniformly) at frequencies  $f = m \Delta f$ , the total number of samples is  $N_{max}$ , and the various parameters are related by the equality  $\Delta t \Delta f = 1/N_{max}$ .)

- 9.5) Figure 12 shows three traces of the noise spectral density, obtained from the same erased track at three different disk velocities. According to Eq. (46) the Modulation Transfer Function (MTF) should not affect the low-frequency end of the spectrum, yet the DC noise level in the figure drops by about 3 dB for each doubling of the velocity. Clearly, the spectrum  $S_{\psi_0}(f)$  of the signal itself is responsible for the observed behavior. Explain this phenomenon on the basis of the definition of the spectral density function in Eq. (16).

## References

1. J. Smith, *Modern Communication Circuits*, McGraw-Hill, New York, 1986.
2. A. Papoulis, *Probability, Random Variables, and Stochastic Processes*, 2nd edition, McGraw-Hill, New York, 1984.
3. A. Arimoto, M. Ojima, N. Chinone, A. Oishi, T. Gotoh, and N. Ohnuki, "Optimum conditions for the high frequency noise reduction method in optical videodisc players", *Applied Optics* 25, pp1398-1403 (1986).
4. M. Ojima, A. Arimoto, N. Chinone, T. Gotoh, and K. Aiki, "Diode laser noise at video frequencies in optical videodisc players", *Applied Optics* 25, pp1404-1410 (1986).
5. G. A. Acket, D. Lenstra, A. J. Den Boef, and B. H. Verbeek, "Influence of feedback intensity on longitudinal mode properties and optical noise in index-guided semiconductor lasers", *J. Quant. Elect. QE-20*, pp1163-1169 (1984).
6. A. G. Dewey, "Optimizing signal to noise ratio from a magneto-optic head", paper EO8.2, presented at the meeting of the Optical Society of America, Boston, Massachusetts, November 1990.
7. A. G. Dewey, "Optimizing the noise performance of a magneto-optic read channel", *SPIE Vol.1078*, pp279-286 (1989).
8. J. W. Beck, "Noise considerations in optical beam recording", *Applied Optics* 9, pp2559-2564 (1970).
9. J. P. J. Heemskerk, "Noise in a video disk system: experiments with an (AlGa)As laser", *Applied Optics* 17, pp2007-2012 (1978).
10. F. Inoue, A. Maeda, A. Itoh, and K. Kawanishi, "The medium noise reduction by intensity dividing readout in the magneto-optical memories", *IEEE Trans. Magnet.* 21, pp1629-1631 (1985).
11. D. Treves and D. S. Bloomberg, "Signal, noise, and codes in optical memories", *Optical Engineering* 25, pp881-891 (1986).
12. A. G. Dewey, "Measurement and modeling of optical disk noise", *SPIE Vol.695*, pp72-78 (1986).

## Figure Captions

- Fig.1 Schematic diagram of a magneto-optical readout system. In the forward path the leaky PBS provides a fraction  $\gamma^2$  of the  $X$ -polarized light to the monitor of laser power. In the return path, 100% of the magneto-optically generated  $Y$ -component of polarization plus the fraction  $\gamma^2$  of the returning  $X$ -polarized light are deflected towards the differential detection module.
- Fig.2 Complex plane diagram showing the locus of  $1+\delta_e(t)$ , where  $\delta_e(t)$  is a small complex quantity whose phase can assume arbitrary values in the interval  $[0, 2\pi]$ . The radius of the circle which is the upper bound on the magnitude of  $\delta_e(t)$  is exaggerated.
- Fig.3 Spectrum of the combined electronic + shot + laser noise as well as that of the electronic noise alone at the output of a laser power monitor [6]. The operating wavelength is  $\lambda = 680$  nm and the incident light power level is  $380 \mu W$ .
- Fig.4 Spectrum of the combined electronic + shot + laser noise as well as that of the electronic noise alone at the output of a laser power monitor [7]. The operating wavelength is  $\lambda = 830$  nm and the incident light power level is  $39 \mu W$ . Since the spikes on the upper trace were generated by the electronic circuitry within the laser power supply, they were ignored in the noise analysis.
- Fig.5 Measured noise spectra at the differential output of a magneto-optical readout system [6]. The operating wavelength and the light power incident on the disk were  $\lambda = 680$  nm and  $P_0 = 2$  mW, respectively. Other system parameters are given in the text (see Example 5). In (a) the disk was stopped. In (b) the spectrum of an erased track shows little deviation from that of a recorded track (carrier frequency = 8 MHz). The spectrum in (c) was obtained with the light blocked from one of the detectors.

- Fig.6 Measured noise spectra at the differential output of a magneto-optical readout system [7]. The operating wavelength and the light power incident on the disk were  $\lambda = 830$  nm and  $P_0 = 2$  mW, respectively. Other system parameters are given in the text (see Example 6). The traces in (a) were obtained with the light blocked from both detectors (lower trace), with the disk stopped but the light allowed to reach the detectors (middle trace), and with the disk spinning and the light reaching both detectors (upper trace). The track under consideration was recorded with a 4 MHz carrier signal. The spectrum in (b) is similar to the upper trace in (a), but the light in this case was blocked from one of the detectors.
- Fig.7 Computed power spectrum of a 4 MHz, 50% duty cycle, square-wave signal in the absence of jitter and other signal fluctuations. A total of 65536 samples were used in this fast Fourier transform (FFT) computation. The exact duration of the signal waveform was  $33.25 \mu\text{s}$ , which is an integer multiple of the carrier period ( $0.25 \mu\text{s}$ ). The approximate values of the sampling intervals in time and frequency are, therefore, 0.5 ns and 30 kHz, respectively. (The exact values of the sampling intervals are slightly different from those quoted above; these are adjusted to fulfill two requirements : *i*) the duration of the signal in time is an integer multiple of the carrier period, *ii*) the total number of samples is an integer power of 2.)
- Fig.8 Section of a square-wave signal in the time interval  $[0, 2 \mu\text{s}]$ , with jitter magnitude  $\Delta t = 25$  ns. A random number generator is used to select the deviation of each zero-crossing point from its nominal position. The deviations are uniformly distributed in the interval  $[-\Delta t, \Delta t]$ , and the random number corresponding to any given point is independent of that for any other point.
- Fig.9 Spectra of square-wave signals (such as the one shown in Fig. 8) with different amounts of random jitter. The noise density shown here is computed within a 30 kHz bandwidth. (a)  $\Delta t = 3$  ns, (b)  $\Delta t = 5$  ns, (c)  $\Delta t = 15$  ns, (d)  $\Delta t = 25$  ns.

- Fig.10 (a) Section of a square-wave signal in the time interval  $[0, 5 \mu\text{s}]$ . The waveform is free from jitter, but its positive amplitude fluctuates randomly within the interval  $[0.85, 1.00]$ . (b) Spectrum of the signal in (a), showing that the noise appears only at low frequencies. (c) Spectrum of a signal waveform with  $\Delta t = 3 \text{ ns}$  of jitter in addition to positive amplitude fluctuations in the interval  $[0.70, 1.00]$ .
- Fig.11 (a) Section of a square-wave signal in the time interval  $[0, 5 \mu\text{s}]$ . The waveform has  $\Delta t = 3 \text{ ns}$  of jitter, its positive amplitude fluctuates randomly within the interval  $[0.70, 1.00]$ , while its negative amplitude fluctuations are confined to the interval  $[-1.00, -0.70]$ . (b) Spectrum of the signal in (a). (c) Spectrum of the same signal when jitter is increased to  $\Delta t = 15 \text{ ns}$ .
- Fig.12 Measured noise spectra from an erased track on a magneto-optical disk [12]. The traces are obtained from the same track under identical conditions with the exception that the disk velocity is different for different traces. The velocities corresponding to these measurements are  $v_0 = 3 \text{ m/s}$ ,  $6 \text{ m/s}$ , and  $12 \text{ m/s}$ .

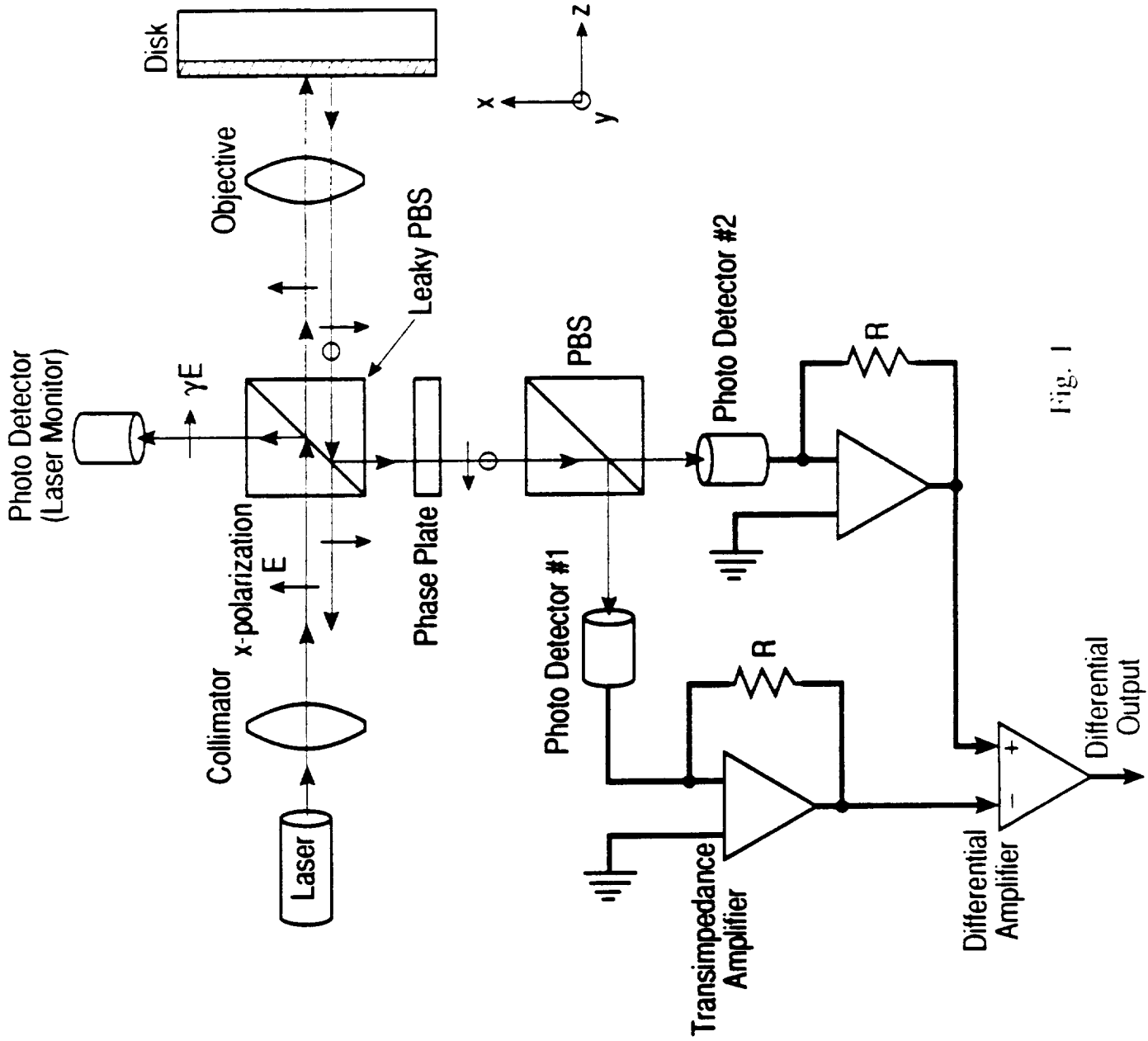


Fig. 1

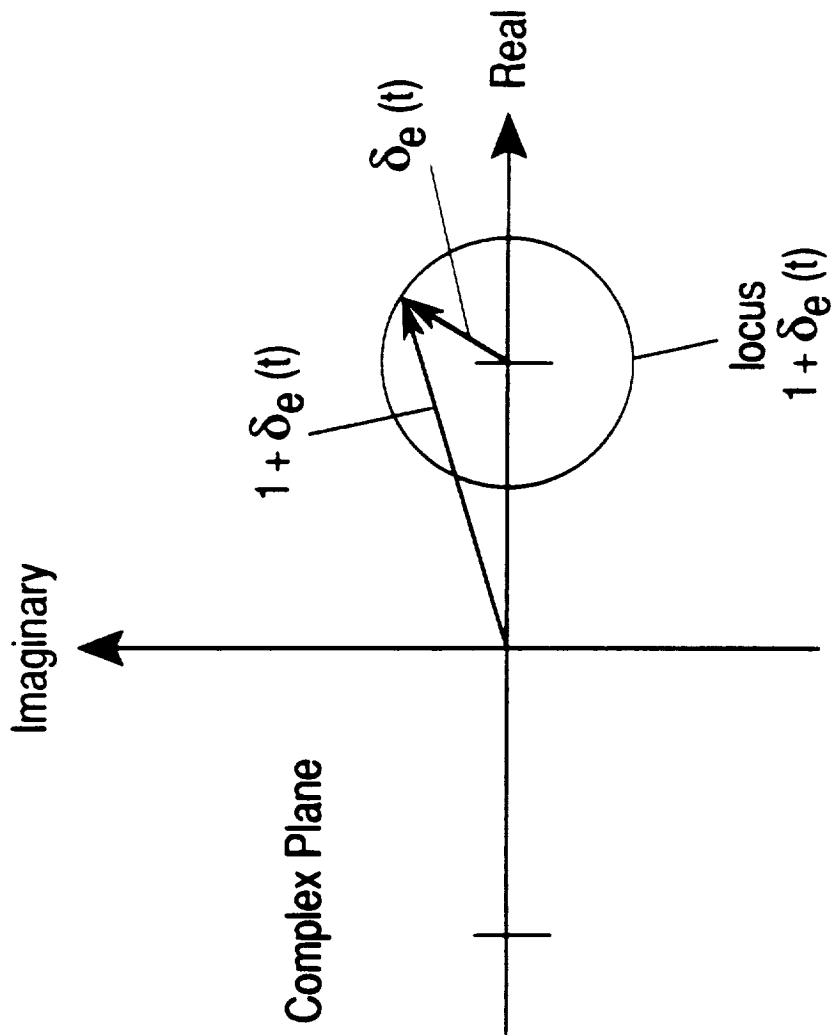


Fig. 2



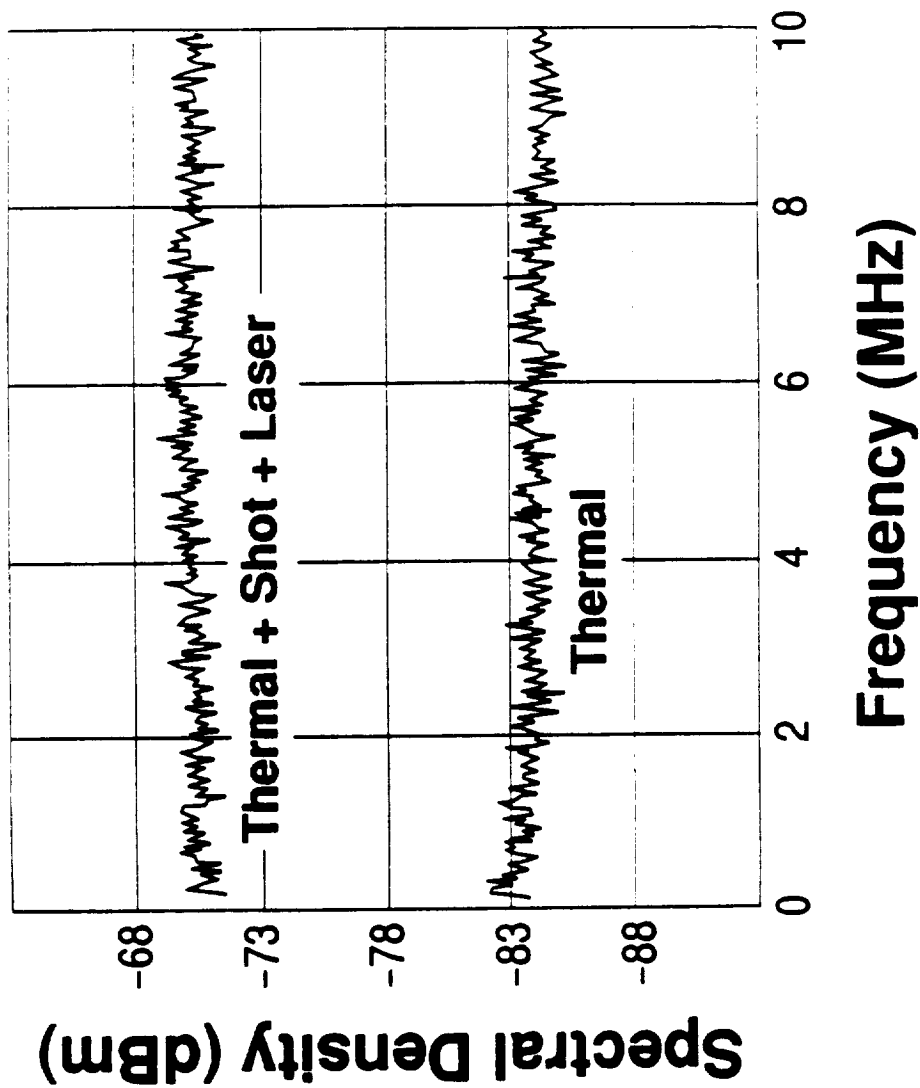


Fig. 3

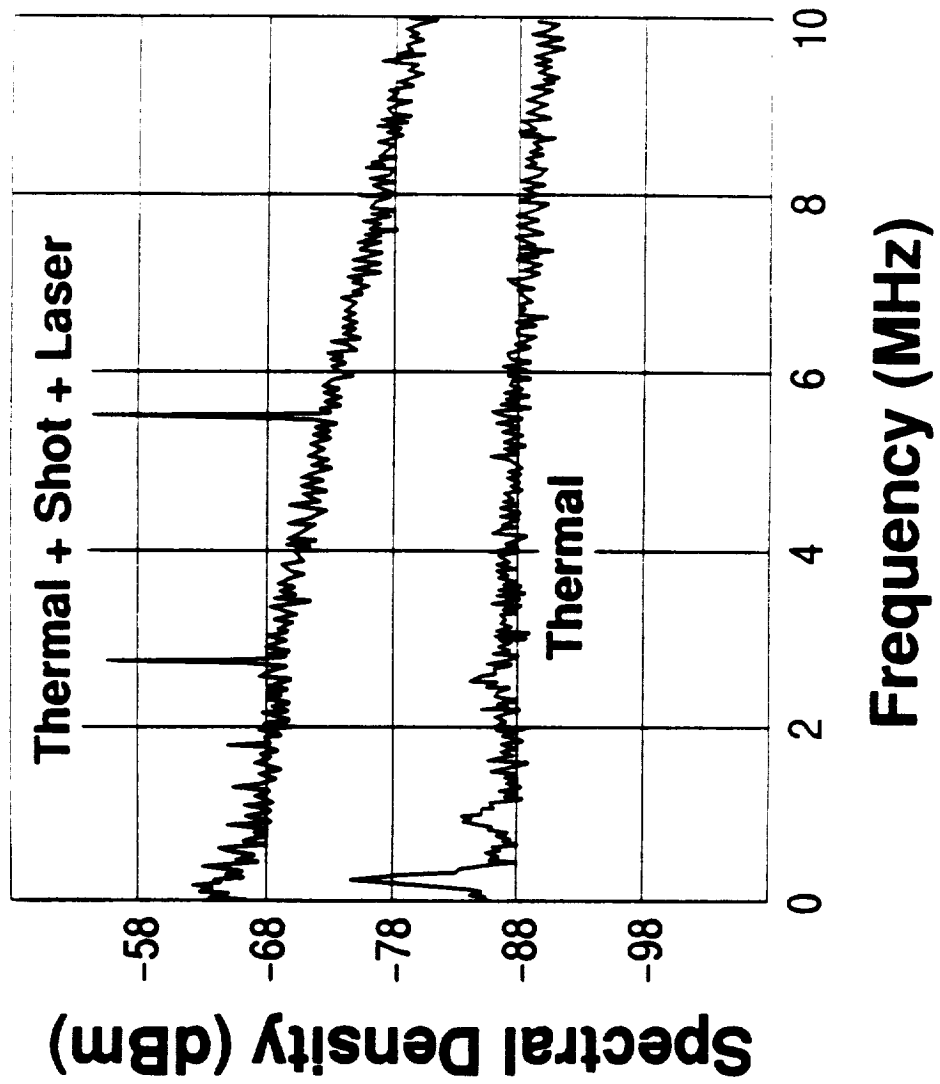


Fig. 4

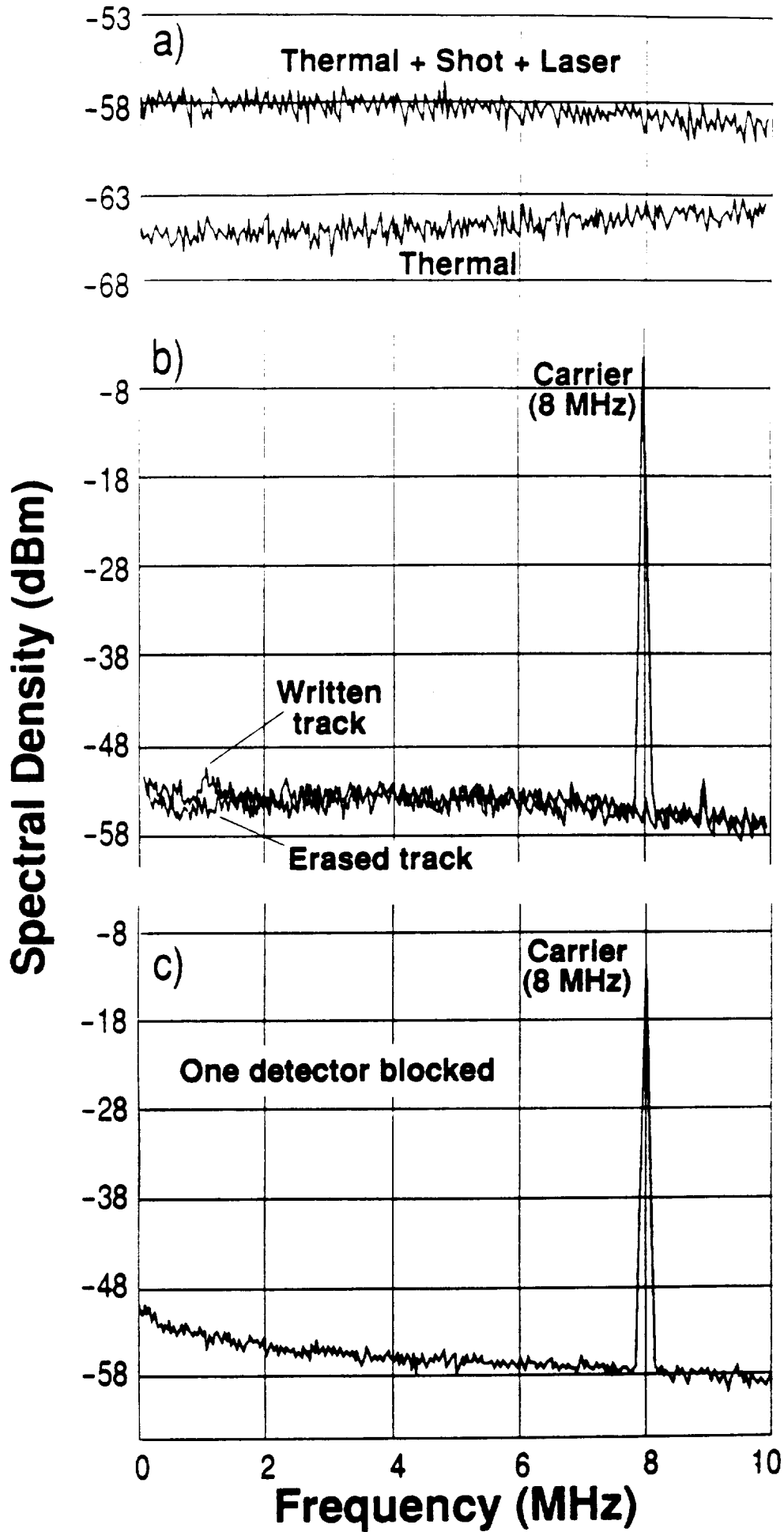


Fig. 5

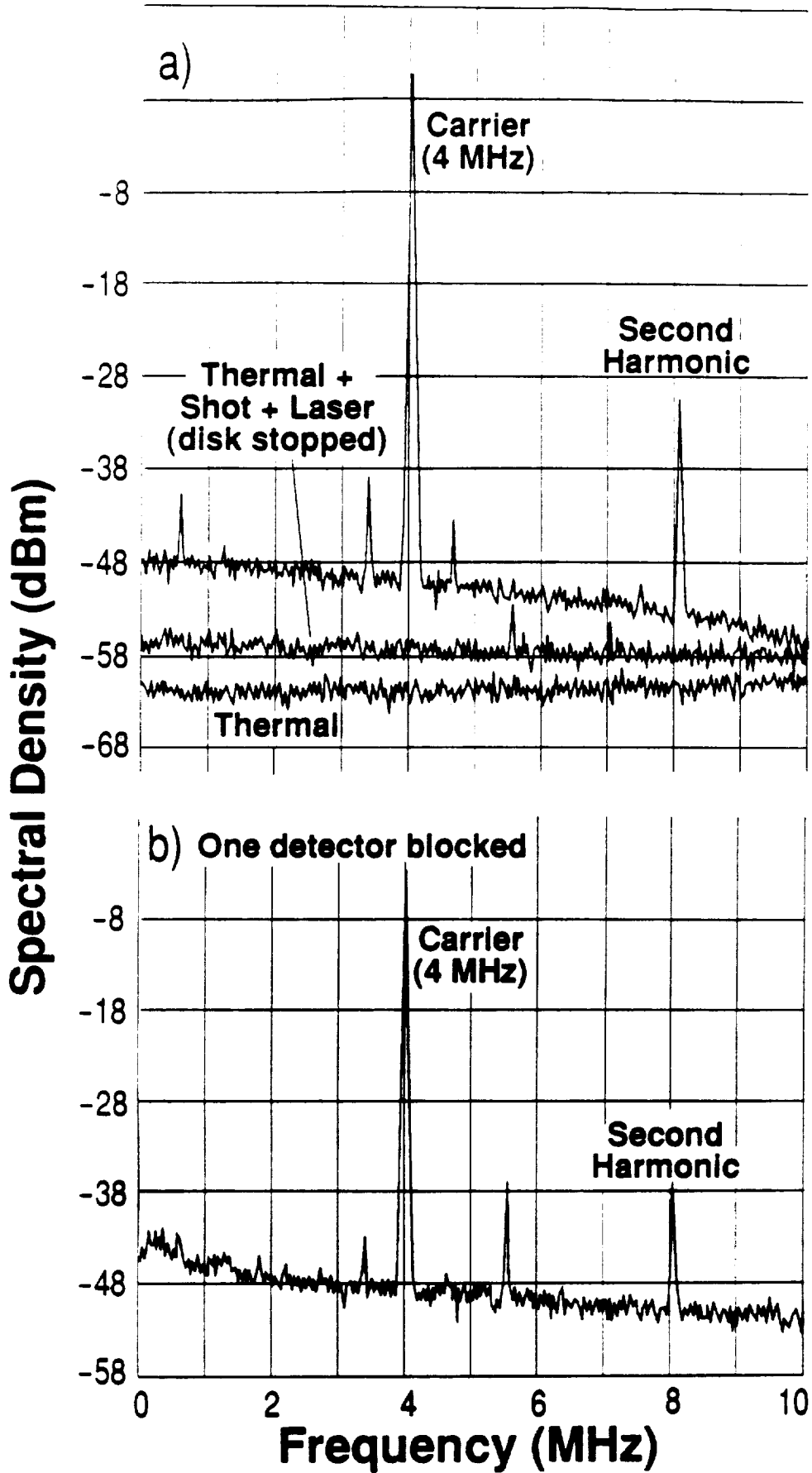


Fig. 6

UA Graphic  
Illustration by Varner  
Manufacturing Co

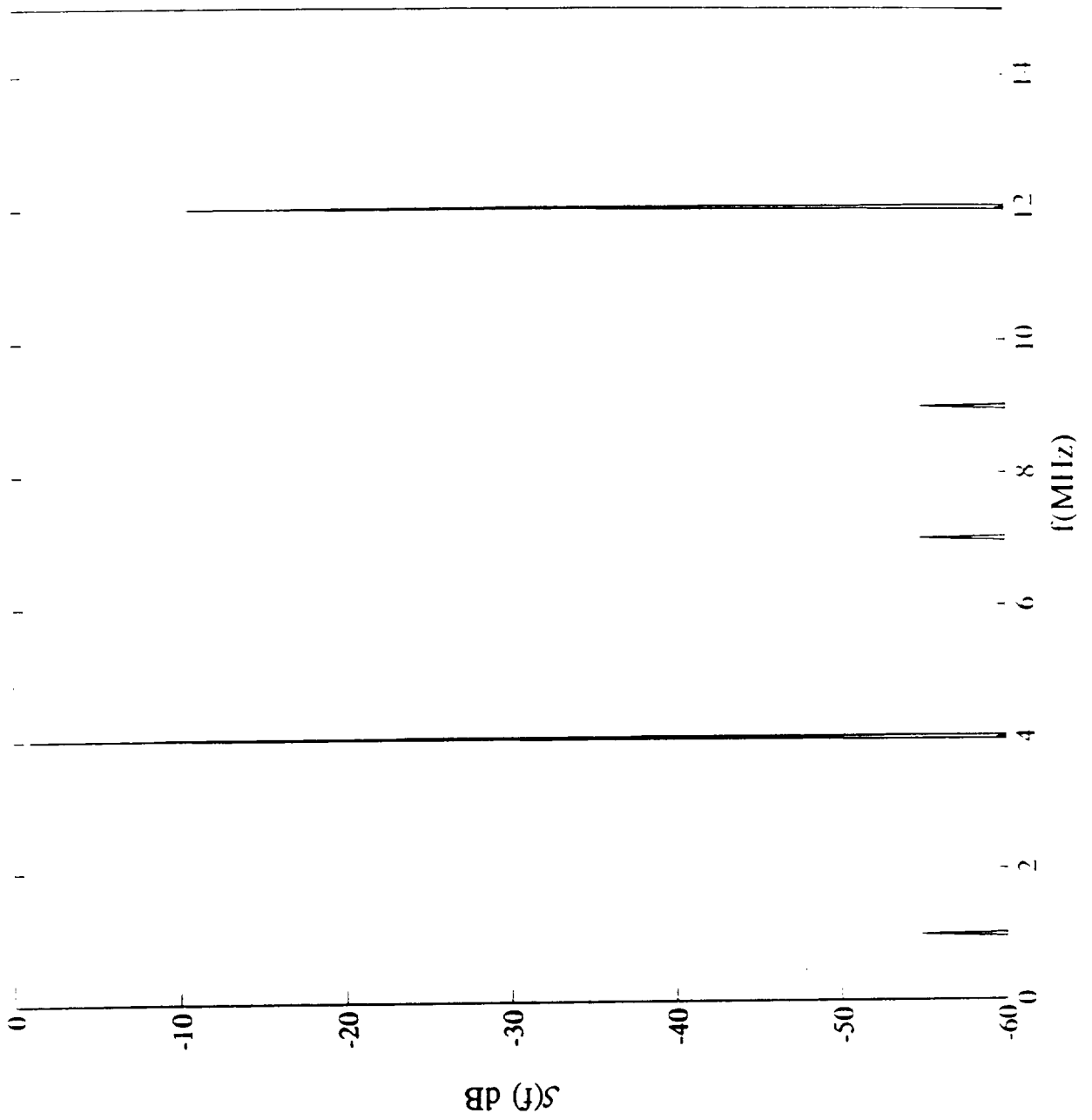


Fig. 7

ORIGINAL PAGE IS  
OF POOR QUALITY

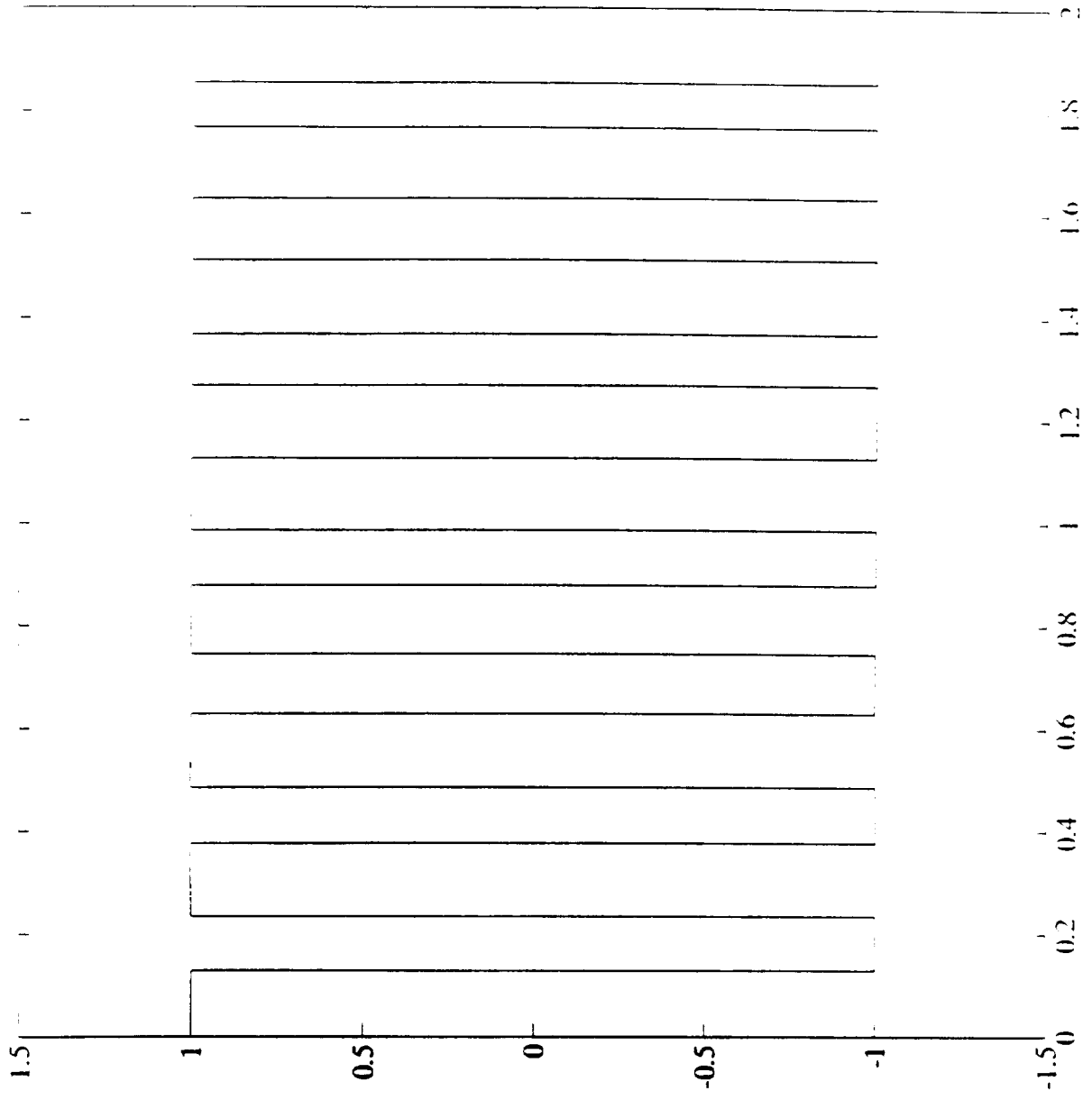


Fig. 8

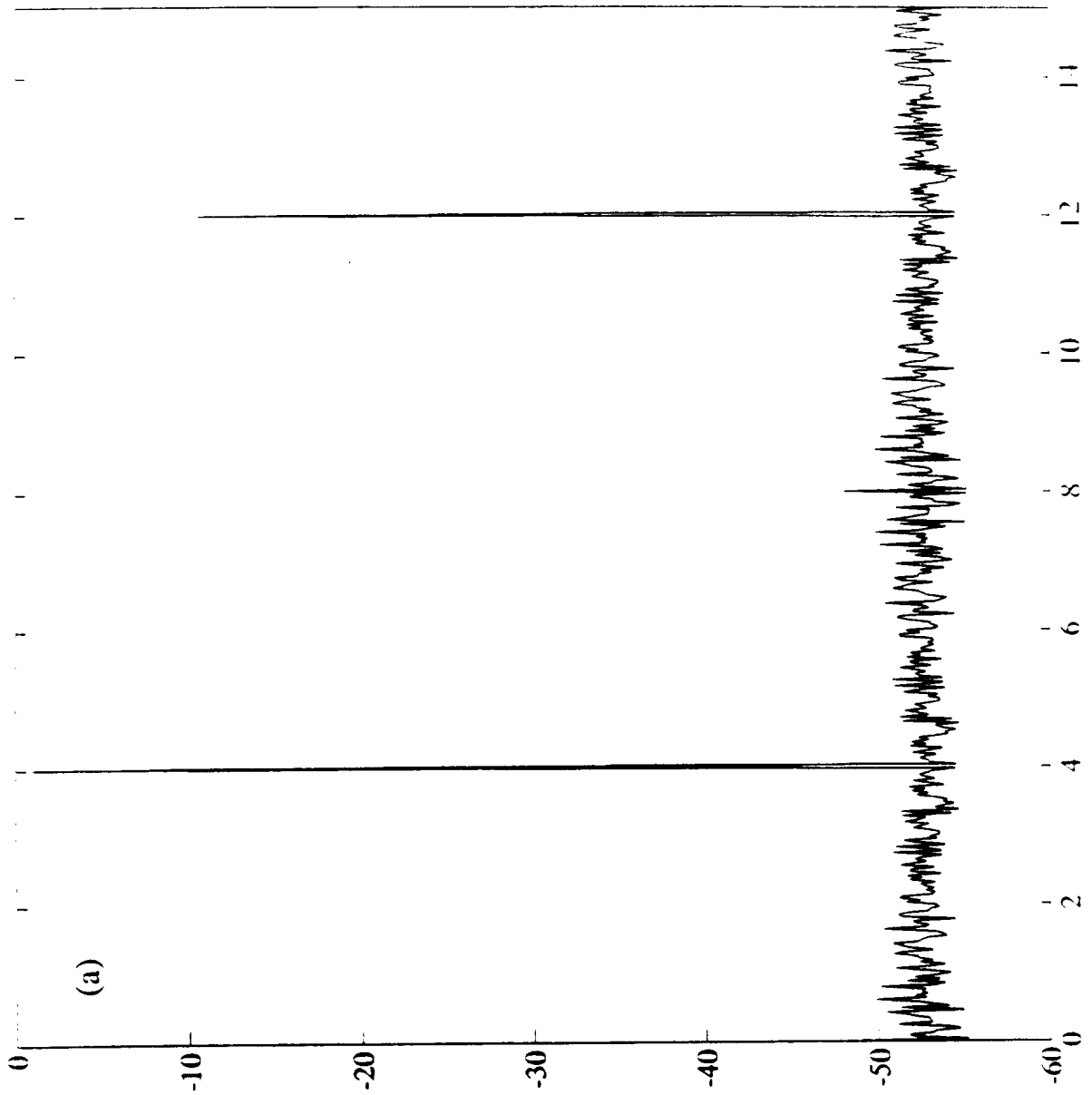


Fig. 9

ORIGINAL PAGE IS  
OF POOR QUALITY

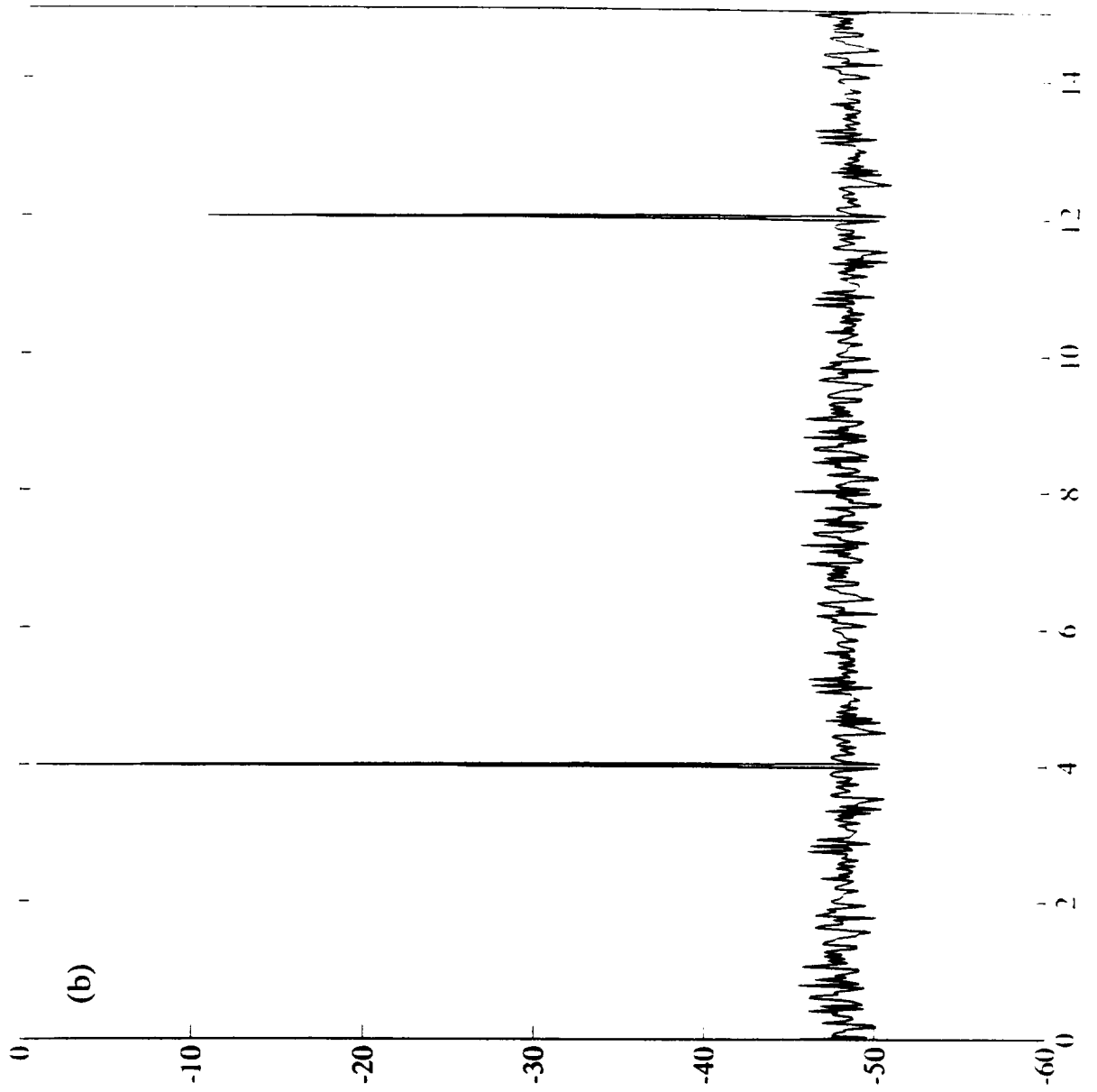


Fig. 9



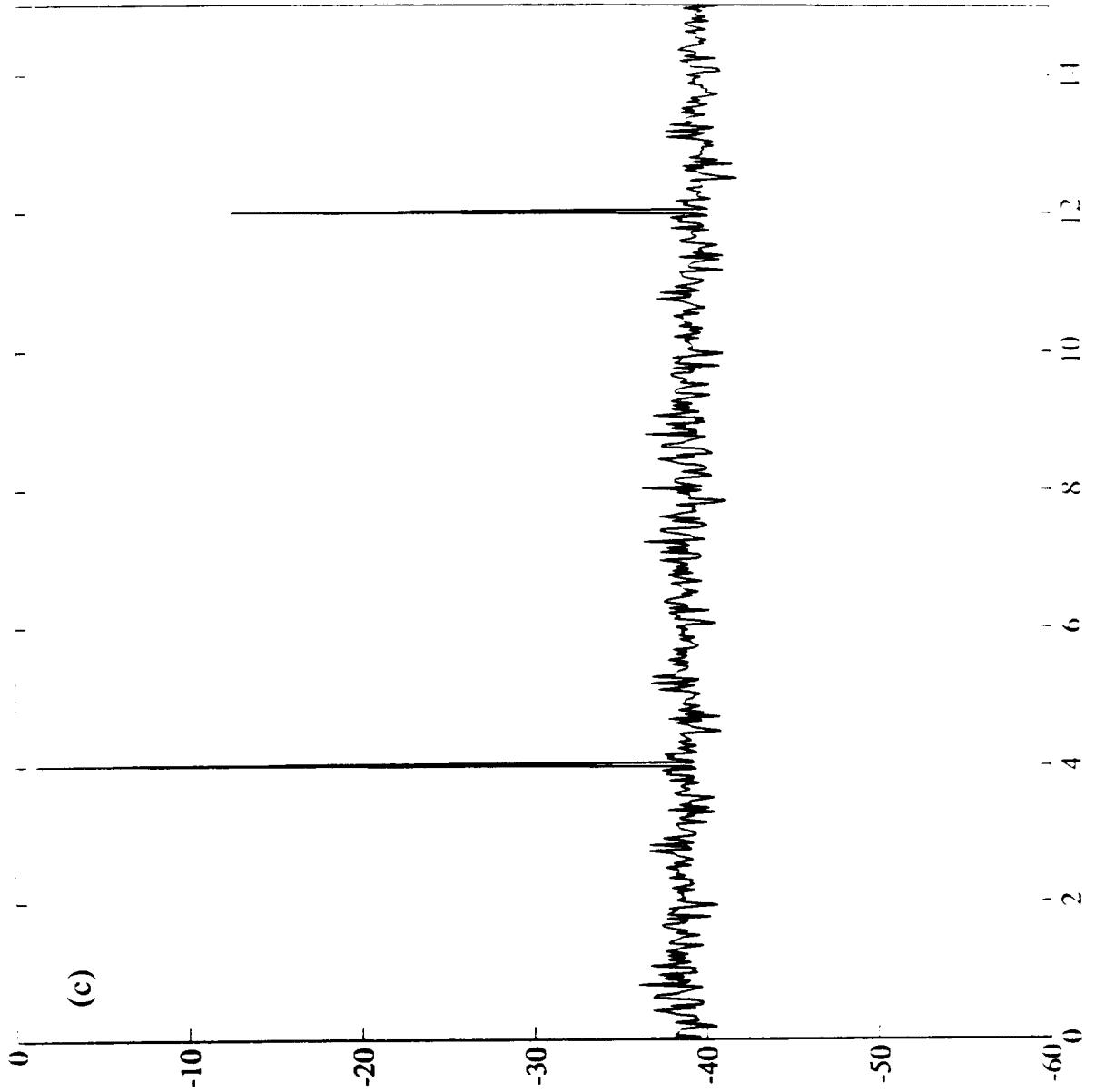


Fig. 9

ORIGINAL PAGE IS  
OF POOR QUALITY

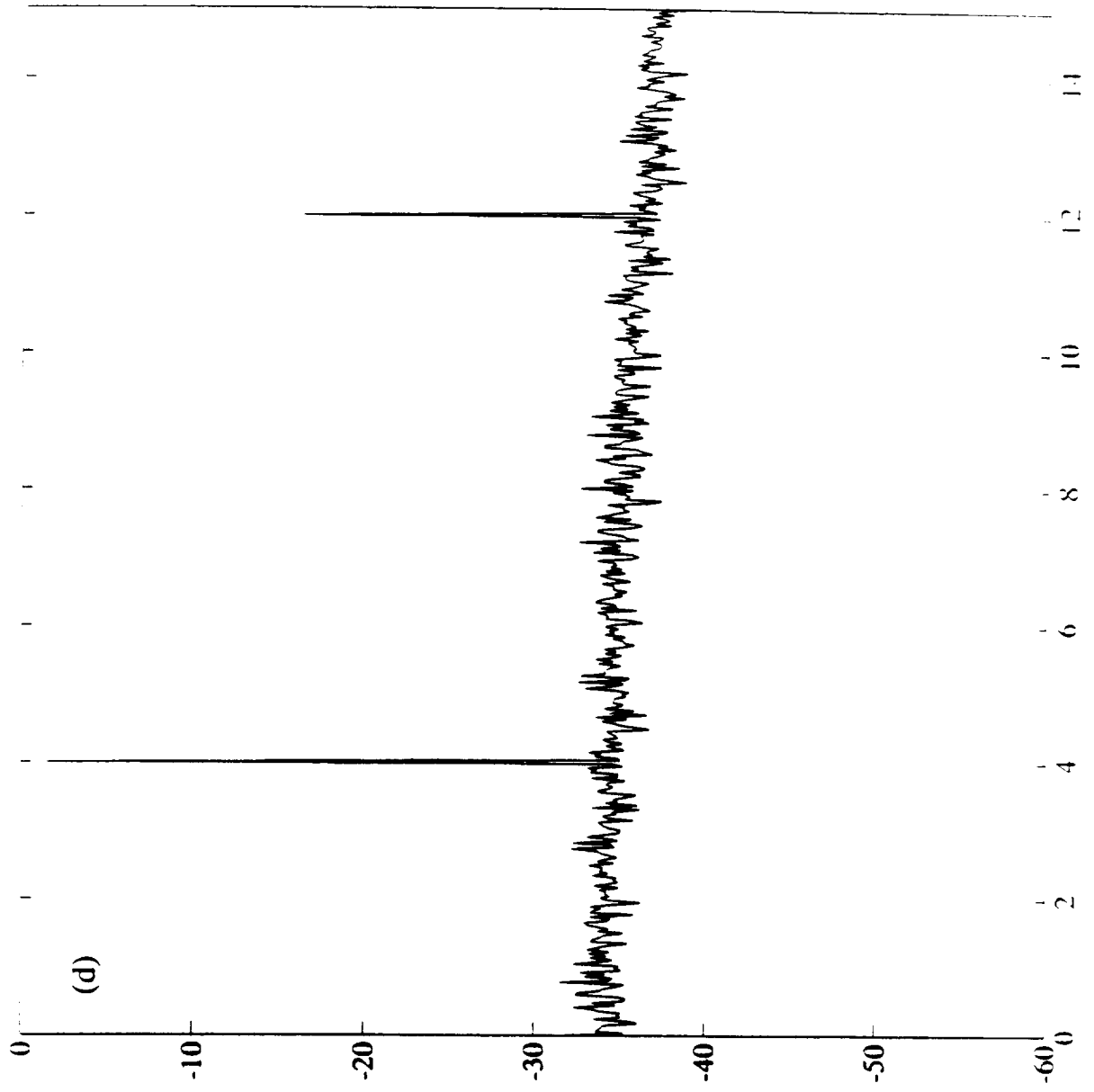


Fig. 9

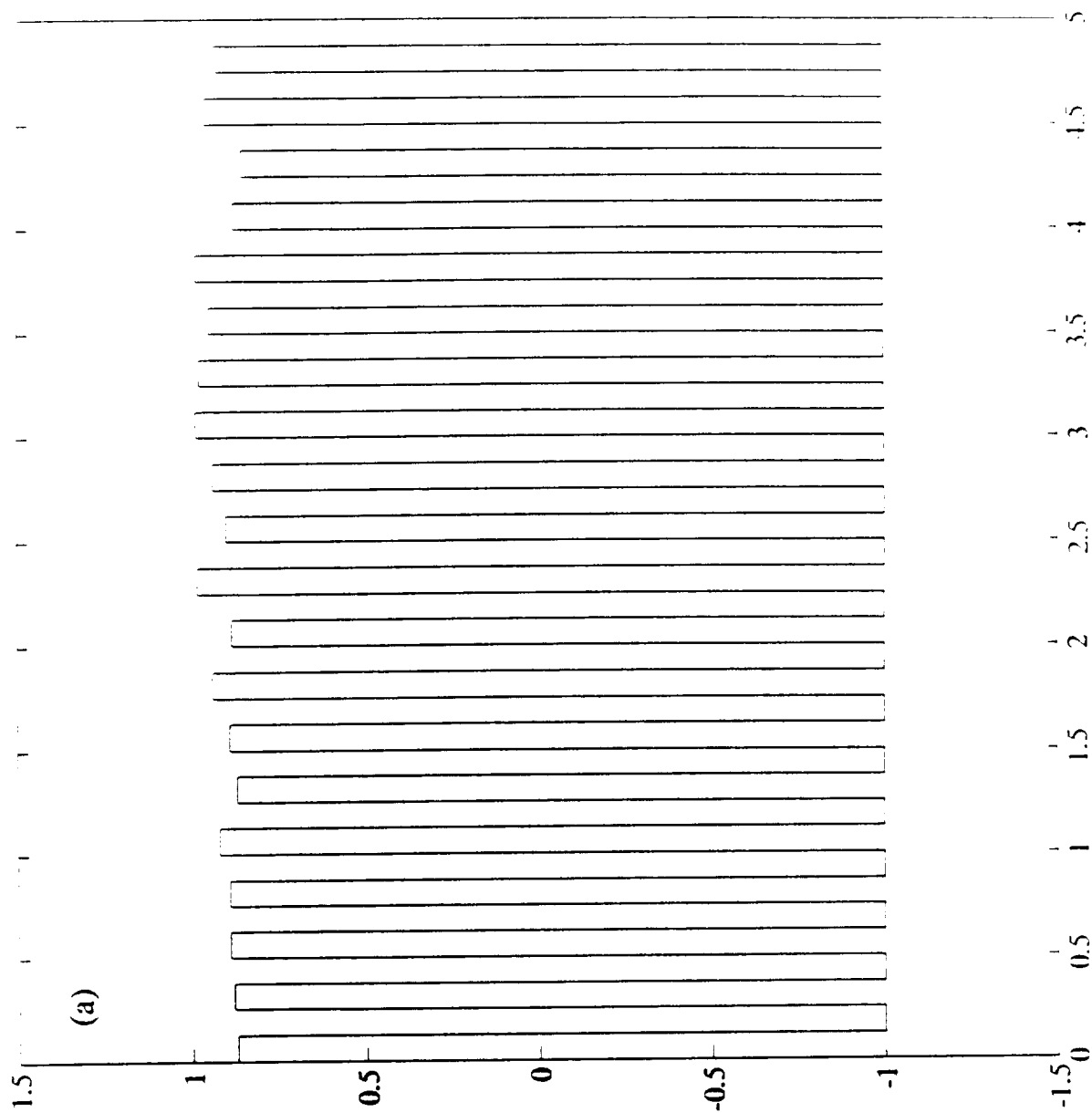


Fig. 10

ORIGINAL PAGE IS  
OF POOR QUALITY

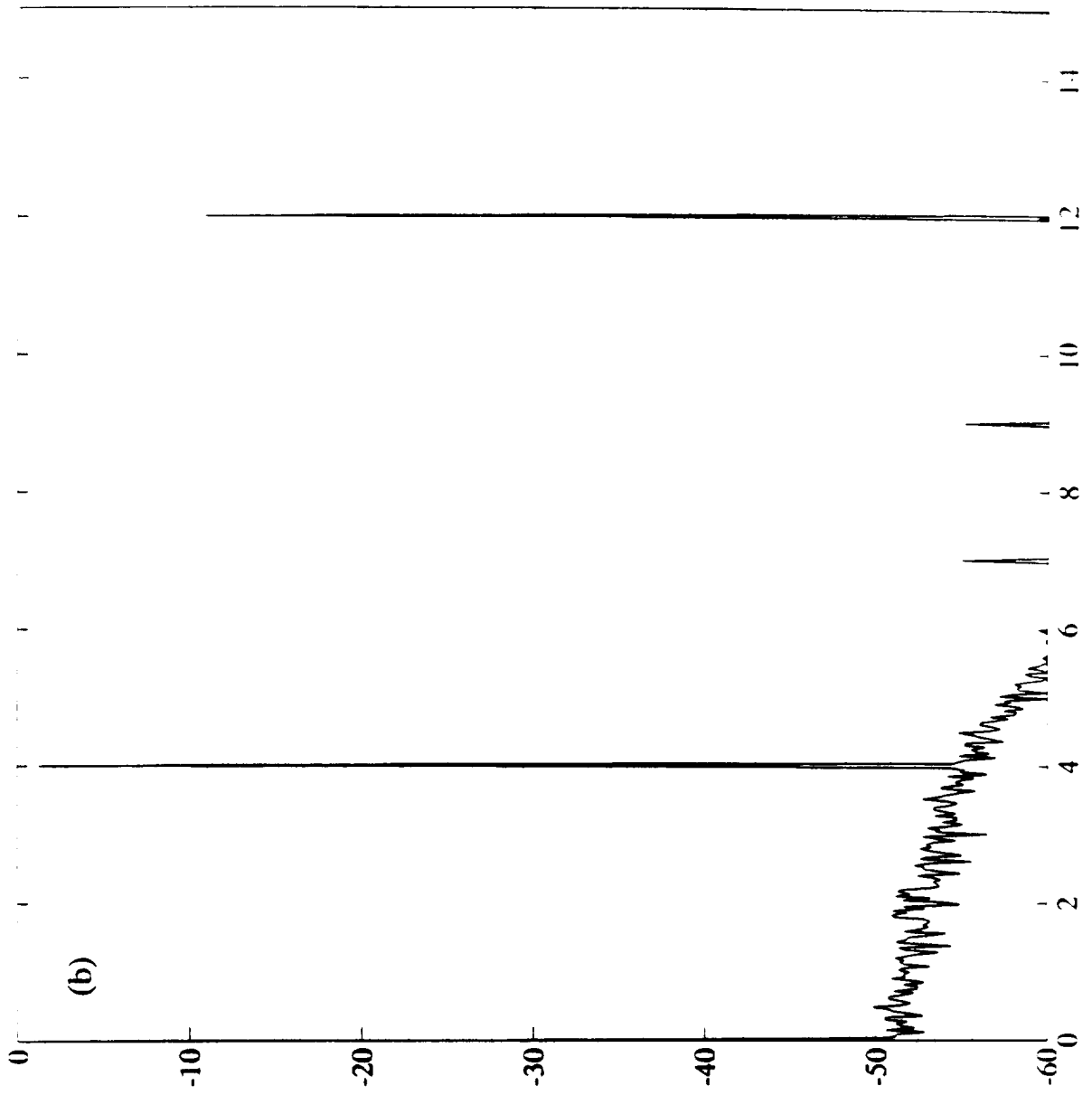


Fig. 10

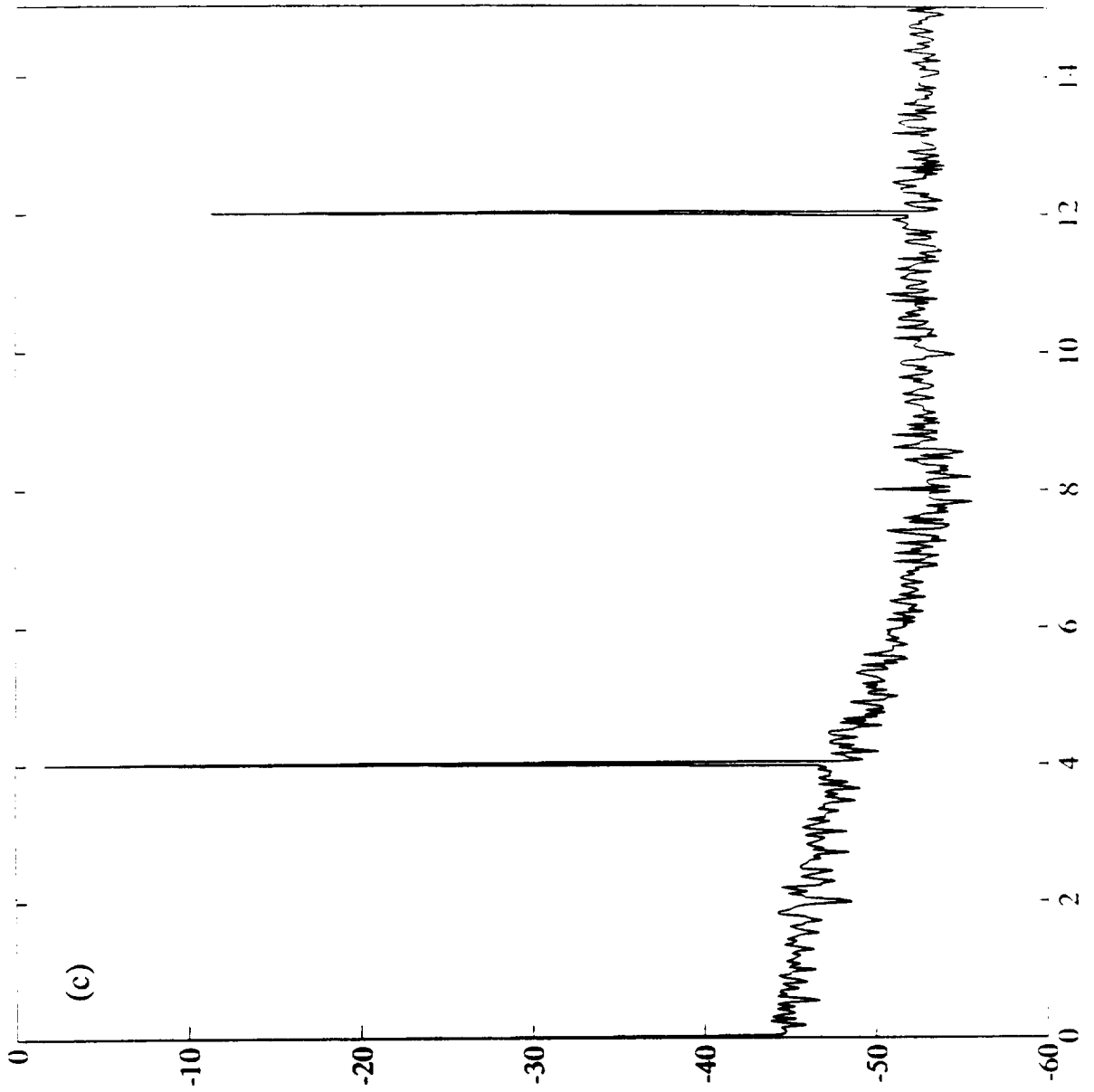


Fig. 10

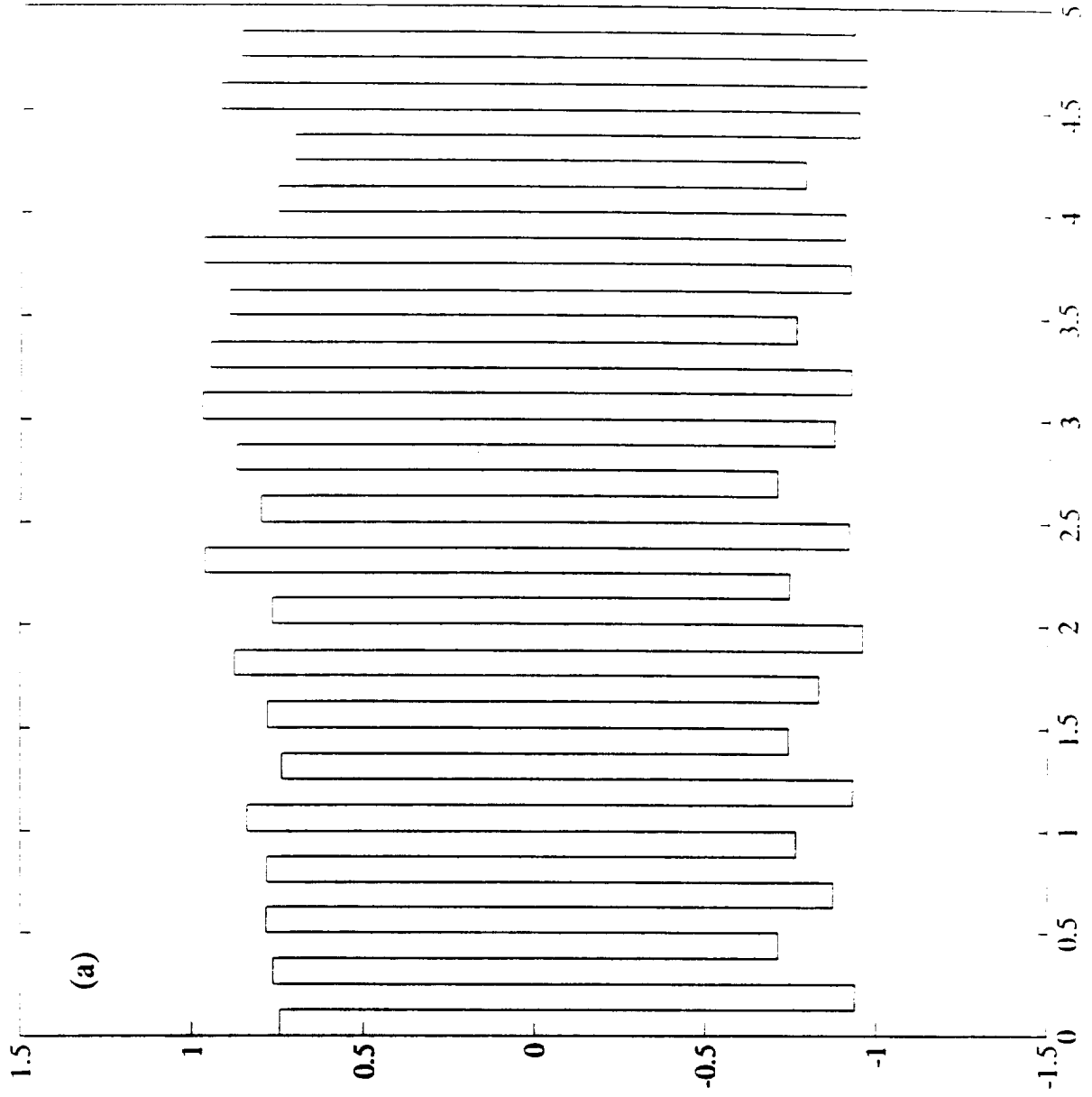


Fig. 11

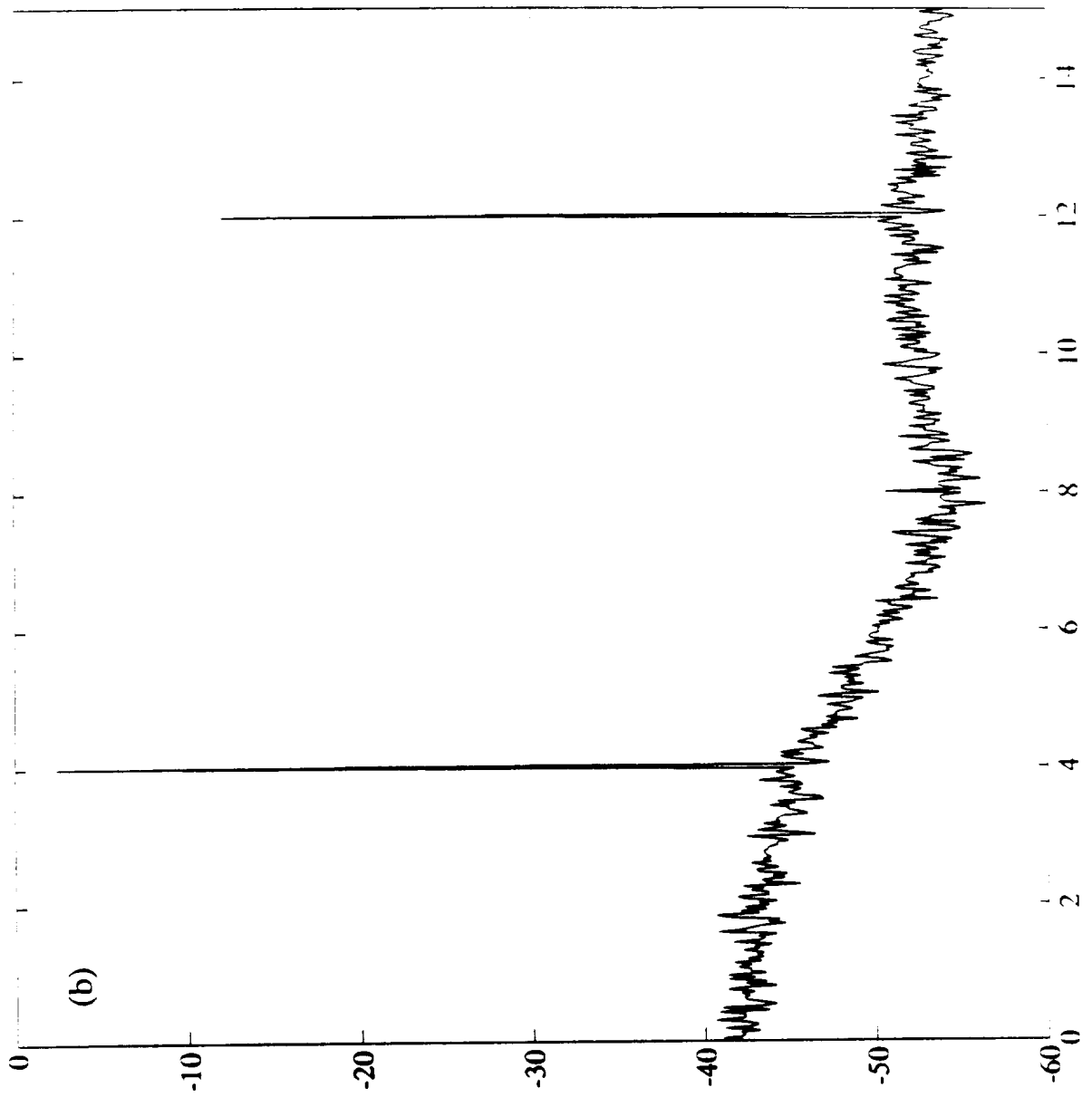


Fig. 11

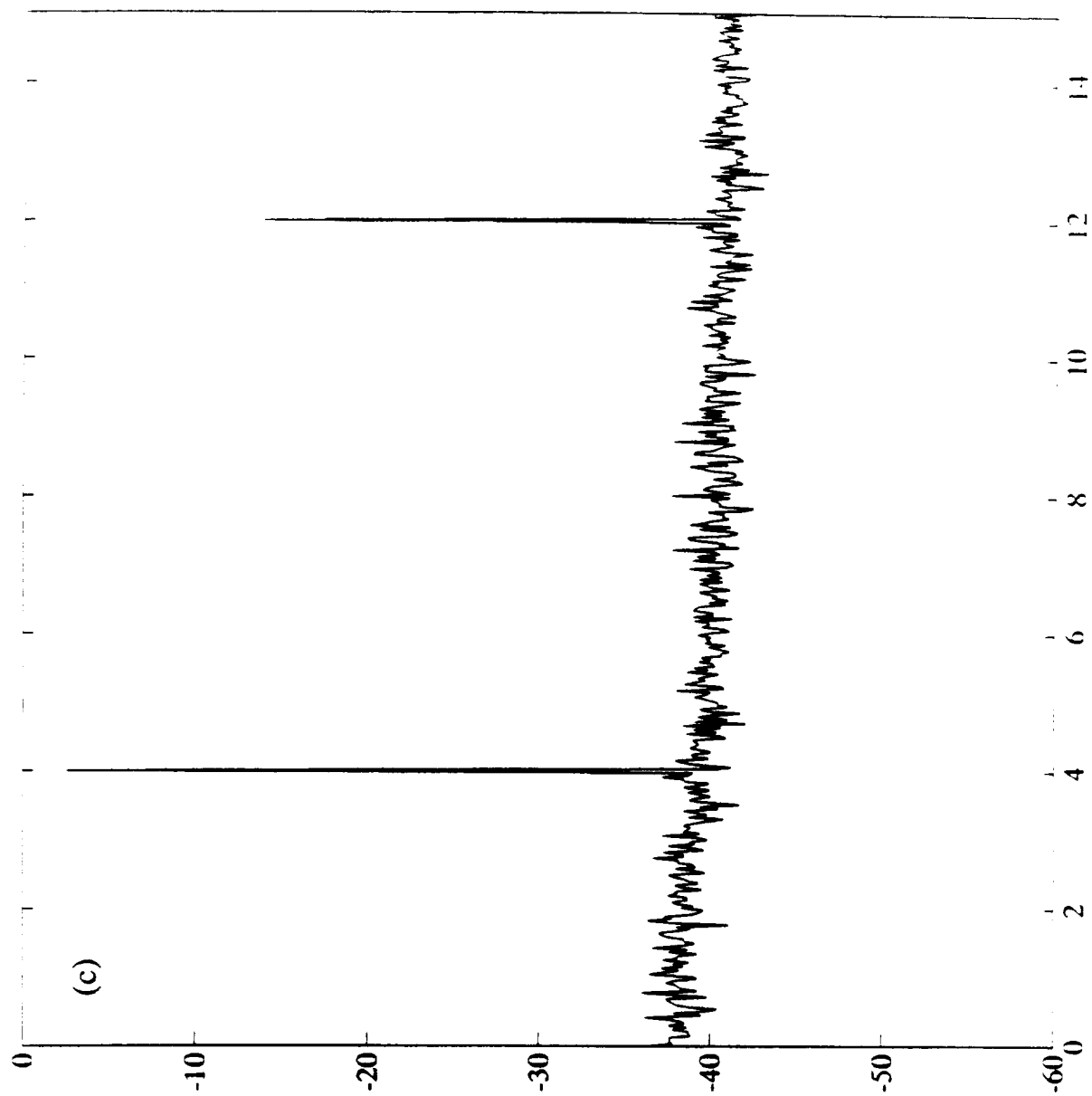


Fig. 11



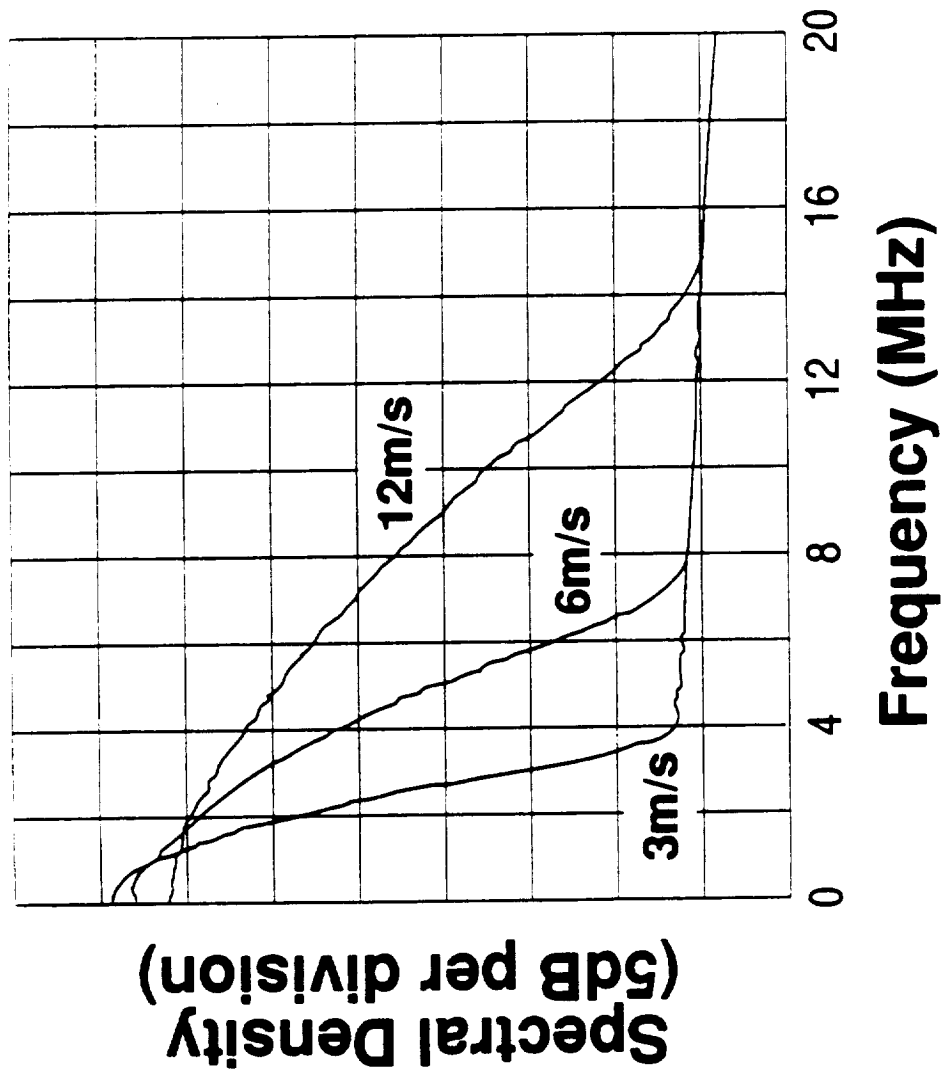


Fig. 12

